Zeitschrift: Archives des sciences et compte rendu des séances de la Société
Herausgeber: Société de Physique et d'Histoire Naturelle de Genève
Band: 37 (1984)
Heft: 2

Artikel: The St. Louis limestone (middle Mississippian) of Illinois basin, USA - a carbonate ramp - bar - platform model
Autor: Diaby, Ibrahima / Carozzi, Albert V.
DOI: https://doi.org/10.5169/seals-740534

Arch. Sc. Genève	Vol. 37	Fasc. 2	pp. 123-169	1984

THE ST. LOUIS LIMESTONE (MIDDLE MISSISSIPPIAN) OF ILLINOIS BASIN, U.S.A. — A CARBONATE RAMP — BAR — PLATFORM MODEL

BY

Ibrahima DIABY and Albert V. CAROZZI [1]

ABSTRACT

The Valmeyeran (Middle Mississippian) St. Louis Limestone of the Illinois Basin was studied through eight cores and six field sections. Detailed petrography of 1542 oriented thin sections led to recognition of sixteen carbonate microfacies. The vertical succession, reciprocal (lateral and vertical) relationships, and correlation coefficients of the microfacies permitted construction of three depositional models.

Model 1 consists of supratidal evaporitic flats (stromatolites, anhydrite, and halite), intertidal to subtidal upper ramp (bioclastic calcisiltites), subtidal lower ramp (mud-supported to grain-supported biocalcarenites) with a crinoidal-bryozoan baffle zone, and basinal environment (mud-supported biocalcarenites and bioclastic calcisiltites).

Model 2 shows the following environments; narrow supratidal evaporitic flats (stromatolites), lagoon (bioaccumulated limestones and biocalcarenites with calcisiltite matrix), subtidal to low intertidal bioclastic bar (biocalcarenites to intraclastic biocalcarenites), slope (biocalcarenites with bioclastic to calcisiltite matrix), and basin (mud-supported biocalcarenites and bioclastic calcisiltites).

Model 3 consists of: still narrower supratidal evaporitic flats (stromatolites), lagoon (calcisiltites, bioaccumulated limestones and biocalcarenites with calcisiltite to bioclastic matrix), oolitic bar-to-bank (oolitic biocalcarenites), slope (biocalcarenites with bioclastic to calcisiltitic matrix), and basinal environment (mud-supported biocalcarenites and bioclastic calcisiltites).

Dolomitization by seepage refluxion of sabkha brines (from supratidal flats) is strong in the upper-ramp calcisiltites of model 1, moderate in the lagoonal calcisiltites of model 2, and minimal in those of model 3.

The three depositional models follow one another in time expressing a progradation of the medium to high energy carbonates towards the depocenter. Near the margins of the basin (SE and E), model 1 was active throughout St. Louis time. Away from the basin edge, model 1 (baffle zone) evolved into model 2 (bioclastic bar) which in turn changed to the oolitic bar-to-bank system of model 3 which remained active till the close of St. Louis time. Probably the depocenter corresponded to a continuous deposition of basinal bioclastic calcisiltites. The succession of these depositional models was extremely rapid, lasting only through two conodont zones.

[1] Department of Geology, University of Illinois at Urbana-Champaign, Urbana, Illinois, 61801, U.S.A. This paper is part of a doctoral dissertation completed by I.D. under the supervision of A.V.C. and submitted to the Graduate College in May 1984.

This research was partially supported by a University of Illinois EXXON gift, a grant from Petróleo Brasileiro S.A. PETROBRAS, and a scholarship from the Ministry of Mines of the Ivory Coast Republic, all of which are gratefully acknowledged. The State Geological Surveys of Illinois, Indiana, and Kentucky are thanked for generously providing the core samples.

The diagenetic features observed petrographically, represent changes that took place in the following environments: marine phreatic, marine vadose, undersaturated freshwater phreatic, saturated freshwater phreatic, mixing marine freshwater phreatic, and burial.

RÉSUMÉ

Le calcaire de St. Louis (Mississippien moyen) du bassin de l'Illinois a été étudié au moyen de huit sondages entièrement carottés et de six coupes stratigraphiques à l'affleurement. L'étude pétrographique détaillée de 1542 coupes minces orientées a révélé la présence de seize microfaciès carbonatés. La succession verticale, les relations réciproques (latérales et verticales) et les coefficients de corrélation des microfaciès ont permis la construction de trois modèles dépositionels.

Le modèle 1 est formé par un platier évaporitique (stromatolites, anhydrite et halite), une rampe supérieure subtidale à intertidale (calcisiltites bioclastiques), une rampe inférieure subtidale (biocalcarénites à grains non jointifs à jointifs) avec une zone de déflection des courants *(baffle zone)* à crinoïdes et bryozoaires, et un milieu de bassin (biocalcarénites à grains non jointifs et calcisiltites bioclastiques).

Le modèle 2 présente les milieux de dépôt suivants: platier évaporitique étroit (stromatolites), lagune (calcaires bioaccumulés et biocalcarénites à matrice de calcisiltite), barre bioclastique subtidale à intertidale profonde (biocalcarénites à biocalcarénites intraclastiques), pente (biocalcarénites avec matrice bioclastique à calcisiltique), et bassin (biocalcarénites à grains non jointifs et calcisiltites bioclastiques).

Le modèle 3 est constitué par un platier évaporitique encore plus étroit (stromatolites), une lagune (calcisiltites, calcaires bioaccumulés et biocalcarénites avec matrice bioclastique à calcisiltique), une barre à banc oolithique (biocalcarénites oolithiques), une pente (biocalcarénites avec matrice bioclastique à calcisiltique), et un bassin (biocalcarénites à grains non jointifs et calcisiltites bioclastiques).

Une dolomitisation par refluxion-filtration des saumures de la sabkha (à partir du platier évaporitique) est forte dans les calcisiltites de la rampe supérieure du modèle 1, modérée dans les calcisiltites lagunaires du modèle 2, et minimale dans celles du modèle 3.

Les trois modèles dépositionels se succèdent dans le temps exprimant une progradation des carbonates d'énergie moyenne à forte en direction du centre de dépôt. Près des bords du bassin (S.E. et E.), le modèle 1 a été actif pendant toute la durée de temps correspondant au St. Louis. A une certaine distance des bords du bassin, le modèle 1 *(baffle zone)* a évolué au modèle 2 (barre bioclastique). Ce dernier à son tour a changé au système de barres et bancs oolithiques du modèle 3. Probablement le centre de dépôt a dû être caractérisé par la sédimentation continue de calcisiltites bioclastiques de bassin. La succession des trois milieux de sédimentation s'est effectuée d'une manière remarquablement rapide pendant la durée de deux zones de conodonts.

Les caractéristiques diagénétiques observées sous le microscope représentent les changements qui ont eu lieu dans les milieux suivants: marin phréatique, marin vadose, eau douce phréatique sous-saturé, eau douce phréatique saturé, mélange phréatique d'eau salée et d'eau douce, et enfouissement.

INTRODUCTION

The purpose of this study is to reconstruct the depositional-diagenetic environments of the St. Louis Limestone on a basinwide scale by determining temporal and spatial relationships of its microfacies. The following approaches were used: detailed field lithologic description and sampling; petrographic investigation which led to the identification of various microfacies; construction of three depositional models; study of the general evolution of the Illinois Basin during St. Louis time, and analysis of the diagenetic processes which affected the rocks.

REVIEW OF PREVIOUS WORK

The St. Louis is generally conformable with the underlying Salem and is overlain also conformably by the oolitic Ste. Genevieve (Figure 1). However local unconformities and lateral transitions exist between the St. Louis and the formations above and below it. As early as 1928, Weller and St. Clair on the basis of field evidence, suggested that in Ste. Genevieve County, Missouri, the base of the St. Louis is gradational; the underlying Salem grading into the St. Louis thereby thickening the latter. Much later, Lineback (1972), using electric logs and drilling samples, showed that in southwestern and south central Illinois, the Salem biocalcarenites grade laterally into the finer grained dolomitic limestones of the St. Louis. In places in

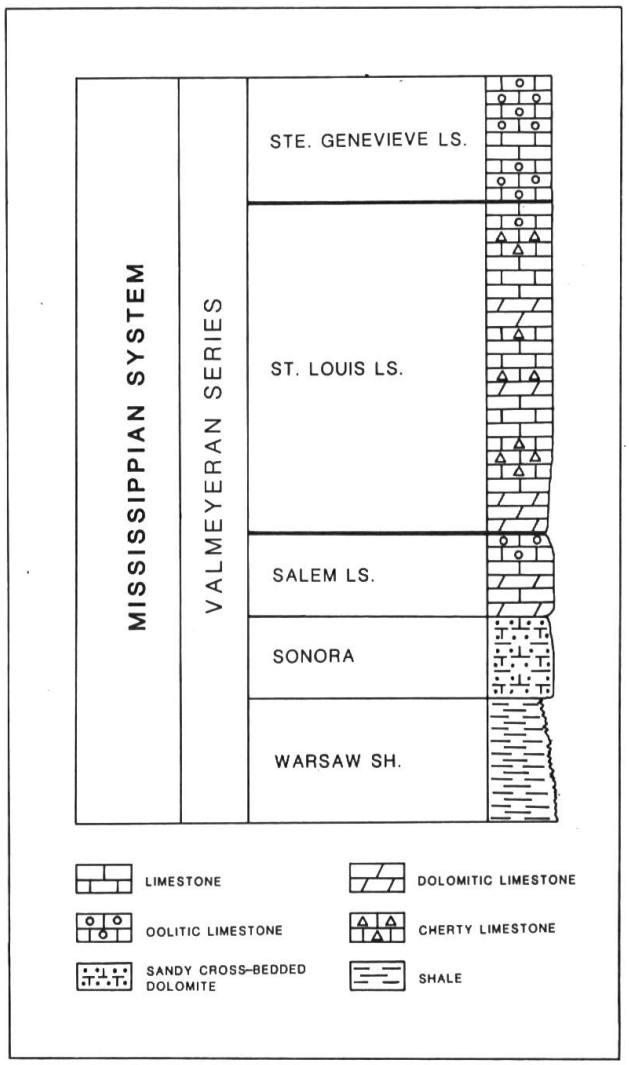

FIG. 1. — Stratigraphic position of the St. Louis Limestone.

western Illinois, the St. Louis rests on the Warsaw Shale or on the argillaceous and dolomitic cross-bedded Sonora Sandstone.

The St. Louis Limestone consists of a lower part of interbedded calcisiltites and dolosiltites with anhydrite beds and collapse breccias, an upper part of biocalcarenites, and a transitional zone of oolitic biocalcarenites at the top of the formation. Krey (1924) described brecciated to conglomeratic limestones in Adams and Hancock Counties, Illinois, and high in the Alton Bluffs. The brecciation is generally attributed to solution of interbedded evaporite units and subsequent collapse of the limestone layers. Patton (1949) in his description of St. Louis lithologies in Indiana, noted all the above mentioned lithologies except the collapse breccias.

Krumbein (1951) and McGregor (1954) were first to rate the occurrence of significant gypsum and anhydrite beds in the St. Louis. Pinsak (1957) found that in the lower St. Louis in Indiana, evaporite beds (generally in three zones) alternate with carbonaceous limestones. Saxby and Lamar (1957) also found an "evaporite zone" in St. Louis cores from southern Illinois. McGrain and Helton (1964) and Dever and McGrain (1969) reported in the St. Louis of Kentucky, anhydrite beds at potentially minable depths.

Rexroad and Collinson (1963) defined two conodont biostratigraphic zones in the St. Louis: the *Taphrognathus* and *Cavusgnathus* zones. In a review of Mississippian microfossils of the Mid-continent region, Baxter and Brenckle (1982) presented a zonation chart. For the zones covering the St. Louis they listed the following foraminifers: *Endothyranopsis*, *Archaediscus*, *Nodoarchaediscus*, *Globoendothyra baileyi*, and the green algae, *Koninckopora inflata*, *K. tenuiramosa* and *K. pruvosti*.

METHODS OF STUDY

Sampling techniques and localities

This study is based on eight cores and six field sections (Figure 2) in the Illinois Basin (Illinois, SW Indiana and western Kentucky). The cores and field sections were selected on the basis of completeness, availability, and relative geographic position within the basin (Diaby, 1984).

The cores and field sections were measured, described and samples were obtained from each macroscopic lithologic unit. A total of 1542 oriented samples were collected from a total thickness of 3073 feet giving an average sampling interval of 2 feet.

An oriented thin section was prepared from each of the 1542 samples. A preliminary subdivision of the thin sections was made on the basis of texture (grain-supported versus mud-supported), matrix, cement, major and minor organic and inorganic components. Subsequently, a quantitative petrographic analysis of each thin section was conducted using the technique of Carozzi (1958, 1961) and expanded

with his coworkers (Stricker and Carozzi, 1973; Kuhnhenn and Carozzi, 1977; Carozzi and Diaby 1981). This method involves measuring indices of clasticity and frequency for both organic and inorganic detrital components. Only frequency is measured for non-detrital benthic and planktic organic components.

The clasticity index of a given component is defined as the mean diameter (in mm) for the six largest grains of that component present in the slide. In this

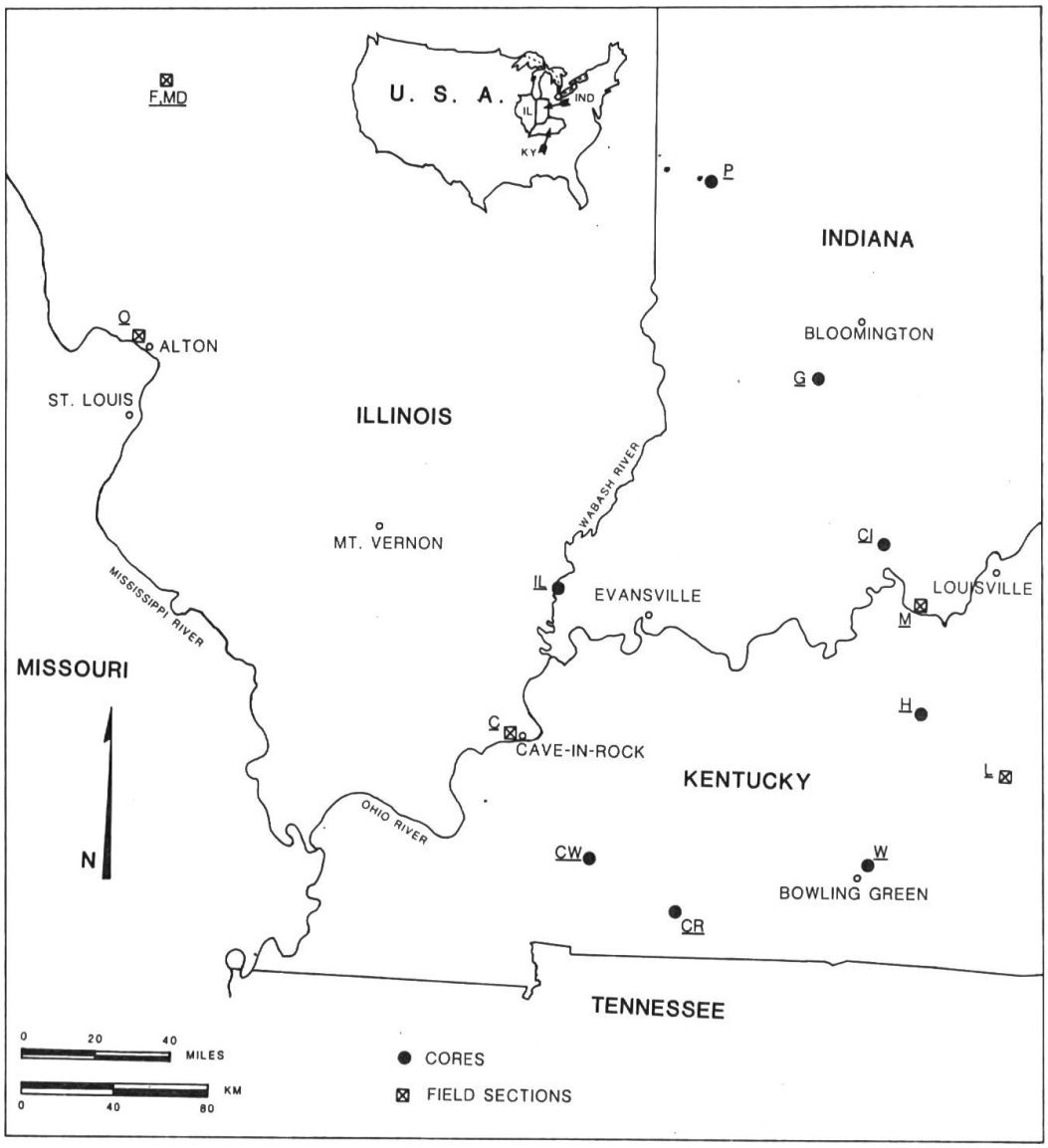

FIG. 2. — Location map of cores and field sections.

Cores: IL: White County, Illinois; P: Parke County, Indiana; G: Greene County, Indiana; CI: Crawford County, Indiana; H: Hardin County, Kentucky; W: Warren County, Kentucky; CR: Christian County, Kentucky; CW: Caldwell County, Kentucky.

Sections: O: Olin Quarry, Alton, Illinois; C: Cave-in-Rock, Illinois; F: Fulton County, Illinois; MD: McDonough County, Illinois; M: Mauckport, Indiana; L: Linwood, Kentucky.

study, clasticity index was measured for the following components: intraclasts, lithic pellets, detrital quartz, fecal pellets, ooids, superficial ooids, and crinoids. These components behave as detrital grains of different densities as all are subrounded and current transported.

The frequency index of a given component is defined as the number of fragments or units of that component within a standard thin section area. In this study, frequency counts were done for the following components: intraclasts, lithic pellets, fecal pellets, ooids, superficial ooids, detrital quartz, crinoids, echinoid spines, bryozoans, *Endothyra*, small foraminifers, brachiopods, calcispheres, sponge spicules, and ostracods. All frequency counts were done within 390 square mm of thin section area corresponding to six low power microscope fields of view.

Intensity of dolomitization and anhydritization was determined by measuring average rhomb or crystal size and by visual estimation of abundance in percentage. Sparite cement, calcisiltite matrix, and bioclastic matrix abundances were also estimated visually.

Relative abundance was estimated for algal laminations, bioturbation, and bioaccumulation with the following adjectives: rare (less than 5%), present (5 to 15%), common (15 to 85%), and abundant (over 85%).

Upon completion of the quantitative petrography, the microfacies were established as distinct entities.

Statistical analysis

The statistical validity of the St. Louis microfacies established above was evaluated with the Iterim subroutine of the iterative classification improvement program of Demirmen (1969) using the IBM 360/75 computer at the University of Illinois. Demirmen's (1969) program uses cluster analysis with calculations of within and between groups sums of squares. The program iteratively recalculates sums of squares for individual observations (thin sections) and compares them to mean sum of squares of the proposed groups. The iterative recalculations (and comparisons) of sums of squares, result in observations (thin sections) being classified in one or another of the proposed groups, hence again affecting the overall within and between groups sums of squares. Provided that the proposed original groups are statistically consistent, the classification will stabilize after a certain number of iterations. A percentage of the thin sections (core ratio) will be retained in their original groups while others may be "rejected" to groups others than the ones to which they originally belonged. In this study, the core ratio was 89% and 11% of the thin sections were "rejected" by the program because they showed local textural variations pronounced enough to affect frequency of components and cause reclassification of these thin sections in microfacies others than the ones to which they were originally attributed. The "rejected" thin sections were returned to their original microfacies because the above textural variations were not found to be geologically

MICROFACIES Components	10	11-12	13	21	22	23	31	32	33	34	35	36	37	38	40	60
Intraclast Freq.	14.20	90.02	24.41	31.06	9.66	14.67	6.36	11.67	1.66	10.95		6.81		4.84		
Intraclast Size	0.50	0.67	0.38	1.27	0.06	0.25	0.10	0.10	0.03	0.09		0.12		0.05		
Pellet Freq.	59.90	105.67	74.00	37.19	95.66	603.25	28.76	83.65	16.30	123.30	16.62	97.30	318.88	184.53	15.00	
Pellet Size	0.04	0.05	0.05	0.03	0.14	0.12	0.02	0.05	0.01	0.07	0.01	0.07	0.07	0.06	0.12	
Ooid Freq.	205.70	175.80	59.40	35.90	7.65			1.62				0.02				
Ooid Size	1.00	0.61	0.69	0.64	0.03			0.01								
Superf. Ooid Freq.	14.40	16.22	0.52	4.87						0.09		0.07				
Superf. Ooid Size	0.31	0.06	0.02	0.10						0.01		0.01				
Crinoid Freq.	74.95	176.88	103.15	142.44	380.66	127.59	148.50	184.15	118.70	133.40	106.16	77.7	37.22	52.23	16.00	
Crinoid Size	1.78	1.20	1.15	2.42	0.74	0.69	1.74	1.38	1.57	1.45	1.53	1.11	0.37	0.66	1.10	
Quartz Freq.	0.96	5.24	74.10		8.46	29.86	4.11	0.31	1.39	5.17		12.76	86.60	50.54	13.00	
Quartz Size	0.10	0.09	0.06		0.06	0.05	0.01	0.02	0.01	0.02		0.02	0.02	0.02	0.10	
% Dolomitiz.			1.11		0.36	2.62	0.32	.22	.58	1.67	1.66	2.66	1.33	3.77		
Aver. Rhomb Size			0.23		0.01	0.02	0.01	0.01	0.01	0.02	0.01	0.03	0.21	0.03		
% Anhydritz.	2.70	0.85	0.85	2.43	0.74	0.73	0.83	0.44	0.22	0.85	0.24	0.80	2.44	1.61		
Aver. Crystal Size	0.08	0.06	0.13	0.24	0.04	0.04	0.05	0.02	0.03	0.07	0.02	0.04	0.06	0.09		

TABLE 1.

Average values of components per microfacies

MICROFACIES Components	10	11-12	13	21	22	23	31	32	33	34	35	36	37	38	40	60
Echinoid Sp. Freq.	1.08	2.57	1.11	4.81	0.56	0.51	1.27	1.50	1.33	1.09	1.28	0.22	0.22	0.33		
Bryozoan Freq.	54.13	116.71	59.07	133.20	369.92	41.43	231.03	99.91	181.20	55.99	174.69	65.00	14.66	31.84	9.20	
Endothyra Freq.	10.95	21.40	9.29	9.06	14.20	10.31	12.17	165.05	19.63	23.16	2.95	4.00	3.77	5.45	3.50	
Small Foram Freq.	2.34	2.48	0.33	0.62	2.72	0.08	0.25	0.94	1.15	0.52	0.35	0.20		0.64		
Brachiopod Freq.	15.87	12.69	9.85	17.37	15.85	4.41	14.23	7.72	11.71	7.46	24.34	9.00	4.33	4.50	1.50	
Calcispheres Freq.	0.35	0.93	0.11		8.13	6.86	0.17	0.44	3.74	2.13	0.12	0.88	5.55	7.16		
Sponge Spic. Freq.						0.65				0.16		0.84	95.77	1.08		
Ostracod Freq.	15.52	6.22	16.81	4.44	12.20	28.43	4.06	12.41	9.38	6.89	9.07	10.85	40.55	25.93		
% Sparite Cement	13.48	13.03	4.48	14.75	11.82	6.99	16.79	8.60	4.07	4.60	8.10	3.21	3.00	3.61		
% Calcisiltite Matrix	7.74	6.05	29.85	4.06	7.20	31.57	3.27	16.87	0.18	20.49	22.97	42.44	61.11	60.91	90%	55%
% Bioclastic Matrix		0.36	1.11		0.56		1.56	0.19	25.91	0.25						
Algal laminations														R		A
Bioturbations			P		R	P		R	R	R	R	R	P	P		R
Bioaccumulation												A				

TABLE 1

(continued)

significant. The stromatolites and calcisiltites were not subjected to statistical analysis because they lacked sufficient components for meaningful quantitative comparison with other microfacies.

The SOUPAC (1976) statistical package program was used to calculate average values of all measured parameters in each microfacies (Table 1). These tables were completed by calculation of average values of components for the stromatolites and the calcisiltites. The table of average values of components was in turn used to calculate Pearson multivariate correlation coefficients between the microfacies (Table 2) with SOUPAC (1976).

	10	11-12	13	31	32	21	22	33	23	34	35	36	37	38
10	1.00													
11-12	.85	1.00												
13	.61	.81	1.00											
31	.31	.62	.60	1.00										
32	.29	.59	.61	.67	1.00									
21	.60	.85	.75	.90	.70	1.00								
22	.34	.69	.69	.96	.74	.91	1.00							
33	.92	.82	.58	.53	.34	.71	.52	1.00						
23	.89	.71	.55	.06	.17	.33	.13	.71	1.00					
34	.36	.69	.78	.65	.79	.73	.77	.30	.37	1.00				
35	.23	.49	.48	.88	.54	.77	.83	.45	.01	.53	1.00			
36	.34	.64	.79	.69	.68	.70	.75	.31	.37	.94	.60	1.00		
37	.15	.27	.51	.08	.26	.11	.16	-.04	.47	.63	.03	.69	1.00	
38	.06	.15	.30	.10	.18	.09	.15	-.02	.24	.40	.06	.45	.50	1.00

TABLE 2

Multivariate correlation coefficients of microfacies

The combination of the Pearson multivariate correlation coefficients between microfacies with the study of the vertical superposition of microfacies in the field sections and cores, led to the recognition of three vertical shallowing upward sequences of microfacies which were in turn interpreted horizontally as three distinct depositional models following Walther's Law (1894, *in* Middleton, 1973). The three depositional models followed one another in time and space during the depositional history of the St. Louis and express the evolution from a carbonate ramp to an intertidal carbonate bar and eventually to a carbonate platform.

COMPONENTS

The limit between organic and inorganic clastic components and matrix was set at 50 microns because of the difficulty in identifying and counting grains below this size by means of a conventional petrographic microscope.

Major and minor organic components

The most abundant organic components are: crinoids, echinodermal debris (mostly crinoidal debris, thereafter referred to as crinoids for the sake of brevity), and bryozoans (both fenestrate and cryptostome). Endothyridae, echinoid spines, brachiopod shells and spines, ostracods, and small benthonic foraminifers are common.

Sponge spicules, pelecypods, calcispheres, and trilobites are minor organic components and may occur in association with rare *Koninckopora*, red algae (stachioides), and fragments of corals, probably *Lithostrotionella*.

Inorganic components

Intraclasts, pellets, and ooids are the major inorganic components. Intraclasts are defined as fragments of previously indurated biocalcisiltite sediment larger than 250 microns, subangular with irregular polygonal shapes, and poorly sorted. Lithic pellets are defined as ellipsoidal grains of similar material as the intraclasts and ranging in size from 50 to 250 microns. The fecal pellets are ellipsoidal grains of calcisiltitic material that occur in association with bioturbation tracks. The fecal pellet sizes range from 50 to 250 microns.

Normal ooids have well developed and multiple cortical layers and often display cerebroid structure. The ooid cores, in order of decreasing abundance are: crinoids, intraclasts, detrital quartz, bryozoans, brachiopods, and *Endothyra*. Superficial ooids are common and associated with the ooids. Other less important inorganic components are silt-sized (rarely sand-size) detrital quartz and pyrite pigments.

DESCRIPTION OF MICROFACIES

The numbering system adopted for the microfacies is as follows;

1) The 10's are oolitic biocalcarenites ranging from well sorted grain-supported or pressure welded oolitic biocalcarenite with sparite cement (10) through bioclastic oolitic sparite cemented calcarenites (11 and 12) to oolitic biocalcarenite with calcisiltite matrix (13).

2) The 20's are intraclastic to lithic pelletoidal biocalcarenites ranging from coarse intraclastic and sparite cemented biocalcarenite (21) through lithic pelletoidal sparite cemented biocalcarenite (22) to lithic pelletoidal biocalcarenite with calcisiltite matrix and sparite cement (23).

3) The 30's range from coarse sparite cemented biocalcarenites (31, 32) to bioclastic calcisiltites (37, 38) with, in between, grain-supported biocalcarenite with bioclastic matrix (33), mud-supported biocalcarenites (34, 36), and bioaccumulated bryozoan-brachiopod limestone (35).

4) The calcisiltites are numbered 40 and may be bioturbated or may show collapse brecciation. Locally, beds of very bituminous calcisiltites with abundant scattered small euhedral anhydrite crystals are found and numbered 50.

5) The stromatolites are numbered 60.

Microfacies identified in this study, were classified using the petrographic terminology for carbonate rocks proposed by Carozzi (1983). These microfacies were divided into the following three broad textural groups. The microfacies of each of the three groups are listed below in order of increasing relative energy:

Group 1. Calcisiltites (including stromatolites).

This group consists of calcisiltites sometimes with small anhydrite crystals or fine grained bioclasts of crinoids, bryozoans, and brachiopods. Bioturbation is profuse. Brecciation caused by dissolution of evaporites may be extensive. The stromatolites have abundant micritic matrix and hence have been included with this group. The microfacies of this group in order of increasing relative energy are: 60, 50, and 40.

Group 2. Pelletoidal calcisiltites to bioclastic-intraclastic calcarenites.

These microfacies range from pelletoidal calcisiltites with scattered fine grained bioclasts to pressure welded sparite cemented biocalcarenites that may be intraclastic. The calcisiltite matrix when present is typically bituminous and commonly pelletoidal. The microfacies of this group are in order of increasing relative energy: 37, 38, 36, 35, 34, 33, 23, 32, 22, 31, and 21.

Group 3. Grain-supported oolitic biocalcarenites.

This group consists of ooid-intraclastic calcarenites with calcisiltite matrix to grain-supported sparite cemented oolitic calcarenites. The bioclastic components are: crinoids, bryozoans, brachiopods, and *Endothyra*. The microfacies of this group are in order of increasing relative energy: 13, 12, 11, and 10.

GROUP 1. CALCISILTITES

Microfacies 60 (Plate 1, A)

Stromatolitic bituminous bioconstructed limestone with regularly to irregularly laminated reddish to dark brown algal mats. Intermat calcisiltite laminae contain rare minute bioclasts of crinoids and bryozoans, and irregular fenestral cavities probably caused by degassing of algal mats.

Microfacies 50 (Plate 1, B)

Laminated calcisiltite with abundant small euhedral anhydrite crystals and common pyrite pigments. The matrix is commonly bituminous and rarely pelletoidal. Wavy calcite pseudomorphs after anhydrite are common. Locally, the anhydrite crystals interfere forming poorly developed rosette textures.

Microfacies 40

Bituminous and slightly pelletoidal calcisiltite with scattered sand-size to silt-size bioclasts of crinoids, bryozoans, brachiopods, and ostracods. *Endothyra*, calcispheres and red algae (stachioides) bioclasts are rarely present. Bioturbation is common resulting in concentrations of small bioclasts between burrows infilled with sparite cemented fecal pellets. Aggrading neomorphism into pseudomicrosparite and replacement by dolomicrosparite are common. In the less bioclastic varieties, collapse brecciation develops subsequent to dissolution of evaporites (gypsum, anhydrite, and halite) followed by collapse of the matrix. The intraclasts are spartite cemented.

GROUP 2. PELLETOIDAL CALCISILTITES TO BIOCLASTIC-INTRACLASTIC CALCARENITES

Microfacies 37 (Plate 1, C)

Pelletoidal bituminous calcisiltite with common monaxonic sponge spicules, calcispheres, ostracods, and crinoids. Minor constituents are bryozoans, brachiopods, coral fragments, and benthic foraminifers. Minor interstitial sparite cement, overgrowths on small crinoid fragments, and calcite infilling of bryozoan zooecia and ostracod shells are present. Traces of bioturbation occur as vaguely defined burrows infilled with partly merged fecal pellets.

Microfacies 38

Finely pelletoidal bituminous calcisiltite with common sand-size to silt-size bioclasts of crinoids, bryozoans, ostracods, calcispheres, sponge spicules, and brachiopods. Slight pressure-welding is displayed by deformation of the fecal pellets and the interparticle cement is microsparitic. Small anhydrite crystals and silt-size quartz are sometimes present. There is a faintly laminated fabric resulting from subparallel alignment of elongate bioclasts.

Microfacies 36 (Plate 1, D)

Poorly sorted bioturbated mud-supported biocalcarenite. Bioclasts of crinoids, bryozoans, echinoid spines, and brachiopods occur as floating grains within a calcisiltite matrix. Other less common bioclasts are coral fragments, pelecypods, ostracods, calcispheres, *Endothyra*, and rare small benthic foraminifers. Rare calcisiltite intraclasts and silt-sized detrital quartz are present. The calcisiltite matrix is bituminous with abundant pyrite pigments and is locally pelletoidal.

Microfacies 35 (Plate 1, E)

Bioaccumulated bryozoan-brachiopod limestone with pelletoidal calcisiltite matrix. Minor amounts of crinoids, coral fragments, ostracods, and pelecypods are associated with rare calcispheres, echinoid spines, and sponge spicules. Many bryozoan zooecia are filled with sparite cement. The matrix is commonly bituminous and displays scattered pyrite pigments.

Microfacies 34

Mud-supported crinoid-*Endothyra*-bryozoan calcarenite. The predominant bioclasts (crinoids, *Endothyra*, and bryozoans) are sand-size and poorly sorted. Brachiopods, echinoid spines, *Koninckopora*, coral fragments (probably *Lithostrotionella)*, and ostracods are accessory components. The bioclasts are floating in a bioturbated bituminous calcisiltite matrix containing silt-sized bioclasts of crinoids, bryozoans, ostracods, together with merged pellets and pyrite pigments. The *Endothyra* are commonly infilled with sparite cement.

Microfacies 33 (Plate 1, F)

Mud-supported to grain-supported crinoid-bryozoan-*Endothyra* calcarenite with bioclastic matrix. Other accessory sand-size components are: brachiopod shells and spines, ostracods, gastropods, trilobites, calcispheres, benthic foraminifers, and silt-size detrital quartz. Very rare ooids are present. The matrix is bioturbated and composed of very fine-grained bioclasts of crinoids and bryozoans in a bituminous calcisiltite groundmass with rare pyrite pigments. The matrix composes 15 to 35% of the microfacies.

Microfacies 23 (Plate 1, G)

Grain-supported fine-grained pelletoidal crinoid-bryozoan calcarenite with calcisiltite matrix and sparite cement. Small well-rounded lithic pellets of calcisiltite are abundant and associated with common crinoids and bryozoans. Brachiopods, pelecypods, and calcispheres are present. *Endothyra*, ostracods, echinoid spines, stachioides, silt-sized detrital quartz, and sponge spicules are rare. The crinoidal bioclasts have syntaxial calcite overgrowth that forms most of the sparite cement of the rock and is associated with pressure-solution of all components. Calcisiltite matrix is common and sometimes shows scattered small euhedral anhydrite crystals.

Horizontal lamination is locally disturbed by bioturbation which leads to concentrations of the calcisiltite matrix.

Microfacies 32

Grain-supported crinoid-*Endothyra*-bryozoan calcarenite with calcisiltite matrix and sparite cement. Medium to fine sand-sized bioclasts of crinoids, *Endothyra*, and bryozoans are common with minor fine sand-sized brachiopod bioclasts, echinoid spines, and small foraminifers. Calcisiltite intraclasts are present. The cement consists of syntaxial overgrowths on crinoids and interparticle sparite mosaic. The calcisiltite matrix has an irregular distribution due to bioturbation and is slightly more abundant than the cement. Localized pressure-solution is visible between crinoids.

Microfacies 22 (Plate 1, H)

Grain-supported intraclast-crinoid-bryozoan calcarenite with sparite cement and common pressure-solution. Moderately well sorted subrounded calcisiltite intraclasts, crinoids, and bryozoans are the most abundant components locally associated with *Endothyra*, small benthic foraminifers, ostracods, calcispheres, echinoid spines, and stachioides fragments. All the cement consists of syntaxial overgrowths on crinoids. A very faint lamination is caused bya lignement of bryozoans, crinoids, and echinoid spines.

Microfacies 31 (Plate 2, A)

Coarse grain-supported to pressure-welded crinoid-bryozoan calcarenite with sparite cement and local pressure-solution. The crinoids and bryozoan bioclasts commonly occur with echinoid spines, *Endothyra*, brachiopods, coral fragments (probably *Lithostrotionella*), and ostracods. Minor components are: calcispheres, stachioides, trilobites, and small rounded intraclasts of calcisiltite. Micritization of *Endothyra* and bryozoan bioclasts is common. The cement consists of syntaxial overgrowths on crinoids grading into cavity filling sparite cement.

Microfacies 21 (Plate 2, B)

Coarse, grain-supported crinoid-intraclast-bryozoan biocalcarenite with sparite cement. Large crinoidal fragments, intraclasts of biocalcisiltite, and bryozoans are the most common components. Echinoid spines, brachiopod shells and spines, *Endothyra*, and gastropods are minor components. All the bioclasts and intraclasts are subrounded to rounded. Micritization of the crinoids is common. The cement is intergranular sparite mosaic with some syntaxial overgrowths on crinoids. Pressure welding is rare.

GROUP 3. OOLITIC BIOCALCARENITES

Microfacies 13

Mud-supported to grain-supported crinoid-ooid-intraclast calcarenite with calcisiltite matrix. Crinoids, ooids, and intraclasts of biocalcisiltite are the most common components. The ooids are commonly abraded and broken. Merged pellets, echinoid spines, and *Endothyra* are the next most abundant components. Ooid cores consist of crinoids, bryozoans, and rare brachiopods and detrital quartz. Small foraminifers and trilobite fragments are rare. The rock is commonly bioturbated and patches of cavity filling sparry calcite occur within the burrows.

Microfacies 12

Grain-supported crinoid-intraclast-ooid calcarenite with sparite cement and pressure welding. Crinoids, small well rounded intraclasts of biocalcisiltite, lithic pellets of calcisiltite, ooids, and superficial ooids are the most abundant components. The intraclasts commonly contain authigenic quartz crystals. The crinoidal fragments often have syntaxial overgrowths which are associated with interparticle mosaic cement. Ooids and superficial ooids show evidence of reworking such as breakage, abrasion, or truncation. Ooid cores consist of crinoids, bryozoans, brachiopods, and detrital quartz. Bioclasts of ostracods, echinoid spines, and stachioides are rare accessory components. Small patches of calcisiltite matrix occur throughout the microfacies.

Microfacies 11 (Plate 2, C)

Grain-supported ooid-crinoid-intraclast calcarenite with sparite cement and local pressure-solution. Ooids and superficial ooids display brachiopod, crinoid, bryozoan, or intraclastic cores. Well rounded intraclasts of calcisiltite often with authigenic quartz crystals are present. The minor components are bryozoans, brachiopods, *Endothyra*, and gastropods. Pressure-solution is common and is shown mostly by straight ooid contacts. The cement is mostly intergranular sparite with rare calcite overgrowths on crinoids.

Microfacies 10 (Plate 2, D)

Grain-supported and pressure-welded oolitic calcarenite with sparite cement. Ooid cores are crinoids, brachiopods, intraclasts, bryozoans, and detrital quartz. Minor bioclasts consist of *Endothyra*, brachiopods, ostracods, echinoid spines, and bryozoans. In rare instances, detrital quartz grains and intraclasts of calcisiltite occur. Pressure-solution is shown by straight ooid contacts, chain ooids, and spalling of ooid outer cortical layers. The cement is intergranular void filling sparite mosaic. Pervasive anhydritization of the ooids, bioclasts, and calcite cement is present. The anhydrite occurs as medium to large euhedral to subhedral crystals or is coarsely fibrous when replacing fracture filling calcite cement.

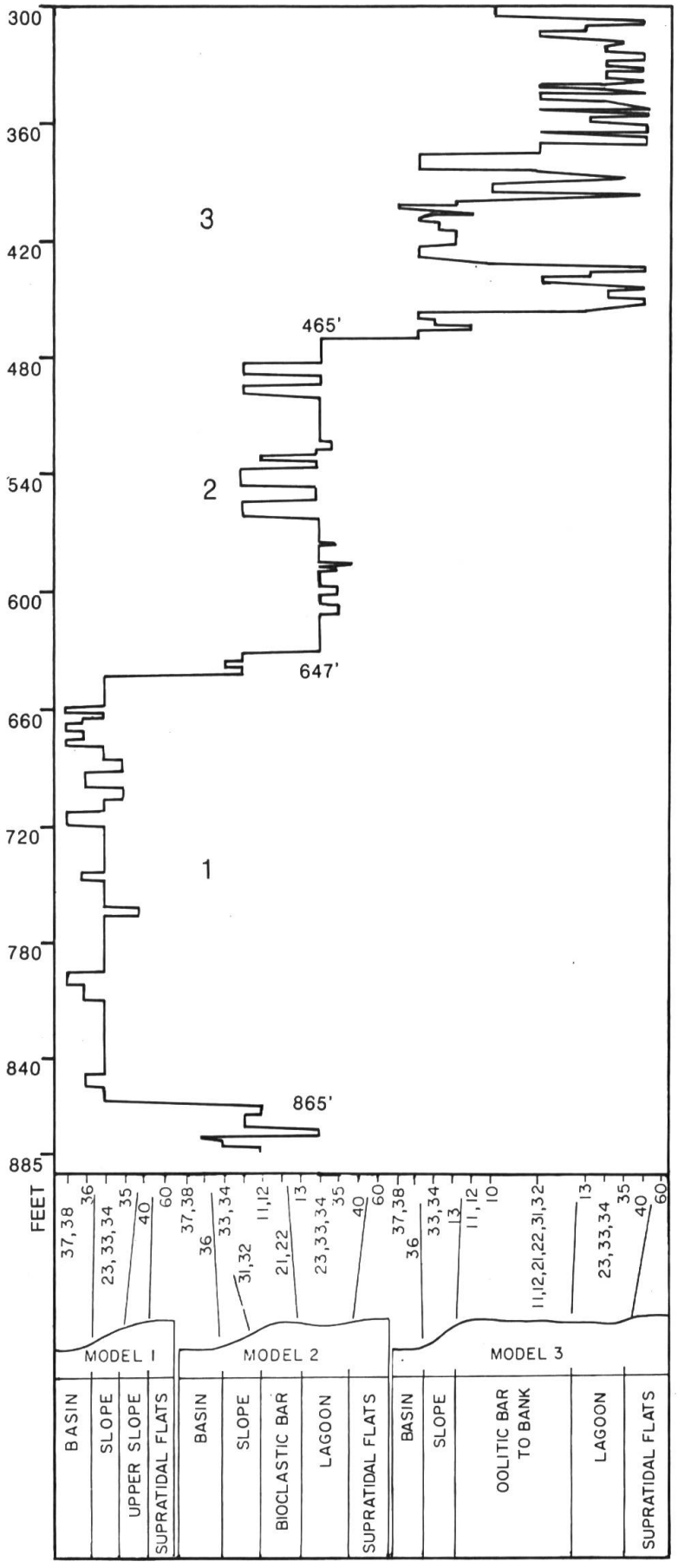

FIG. 3. — Environmental variation curve for Caldwell County core, Kentucky.

DEPOSITIONAL MODELS

MICROFACIES ASSOCIATIONS

The examination of the vertical succession and reciprocal relationships of microfacies shows that three associations of microfacies followed each other vertically in the cores and sections expressing an increasing complexity of the carbonate environments during St. Louis time. These microfacies associations are:

1) A low energy group consisting of microfacies 60, 40, 38, 37, 36, 35, 34, 33, 23.

2) A low and moderate energy group consisting of microfacies 60, 40, 38, 37, 36, 35, 34, 33, 23, 32, 22, 31, 21.

3) A low, medium, and high energy group consisting of the following microfacies 60, 40, 38, 37, 36, 35, 34, 33, 23, 32, 22, 31, 21, 13, 12, 11, 10.

The core of Caldwell County, Kentucky, exemplifies the succession of the three associations of microfacies (Figure 3). Such a distinct evolution requires

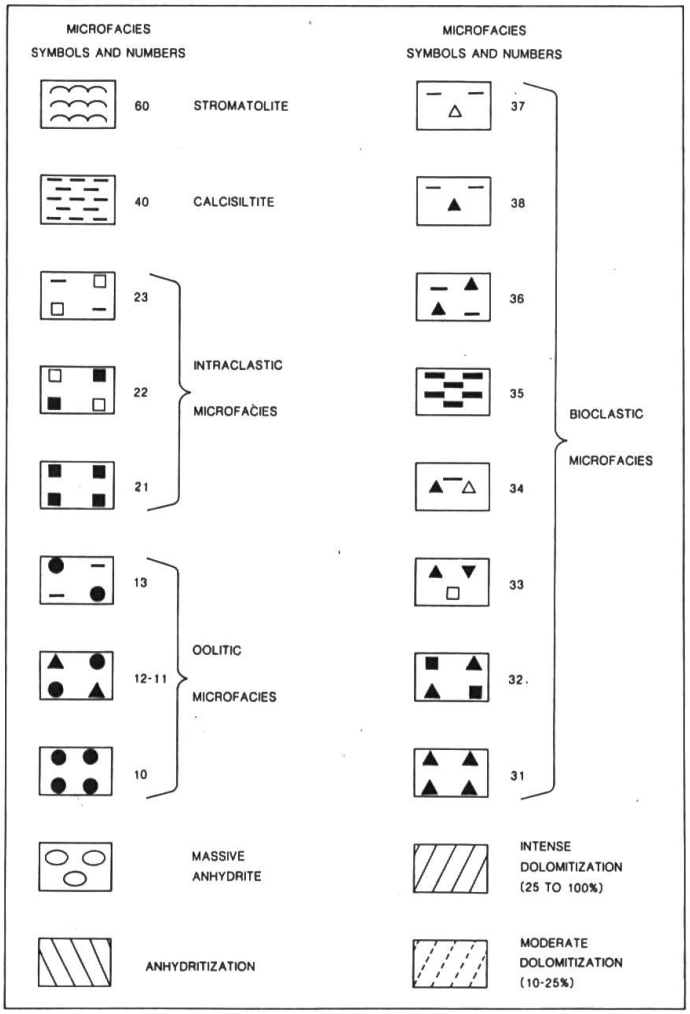

FIG. 4. — Symbols for microfacies and diagenesis for cores and sections.

preparation of three depositional models which followed each other in time. For graphical reasons, the three models are shown as juxtaposed from left to right. The apparent abrupt change from a given model to the successive one results from the fact that the change of model has been arbitrarily located at the first recognized appearance, in a given section or core, of the typical microfacies association of the next model. In reality, the change between successive models is gradual. Each depositional model is first illustrated by an ideal vertical shallowing up sequence with average values of components and a relative depth variation curve at the extreme right (Figures 4, 5, 7, and 9). Each vertical ideal sequence is then transposed into an horizontal depositional model (Figures 6, 8, and 10). The descriptions will be limited to the graphic representation of the latter which consists of curves of average values of component frequencies and clasticities, of average matrix and cement percentages, of relative abundance of certain minor biotic components, textural features, evaporites and dolomitization, and of a relative energy variation curve.

Depositional model 1

Model 1 (Figures 5 and 6) is a gentle carbonate ramp consisting in a basinward direction of the following environments: supratidal evaporitic flats represented by stromatolites (microfacies 60) and laminated evaporite deposits; intertidal to subtidal upper ramp represented by slightly bioclastic calcisiltites (microfacies 40), with fenestral porosity and disseminated minute anhydrite crystals, common collapse breccias due to dissolution of evaporites and flat pebble conglomerates; subtidal lower ramp consisting of mud-supported biocalcarenite (microfacies 34), biocalcarenite with bioclastic matrix (microfacies 33), grain-supported pelletoidal biocalcarenite (microfacies 23), and occasional bioaccumulated bryozoan-brachiopod limestone (microfacies 35); basinal environment represented by a bioturbated mud-supported biocalcarenite (microfacies 36) and bioclastic calcisiltites (microfacies 37 and 38).

The upper ramp is characterized by abnormal low energy, a sparse fauna and pervasive dolomitization represented by small dolomite rhombs scattered in the calcisiltites. This unusual association of features occurs only in model 1. It indicates a restricted hypersaline environment which can be attributed to the combination of the baffling effect of crinoidal buildups of the lower ramp with the seepage refluxion of heavy brines generated by high evaporation rates in the supratidal flats.

Component variations

Crinoids

Maxima of crinoid frequency and size occur in the agitated moderate energy environment of the lower ramp (microfacies 23, 33, and 34) in coincidence with wave-base and representing the peak of energy of this model. From this area of

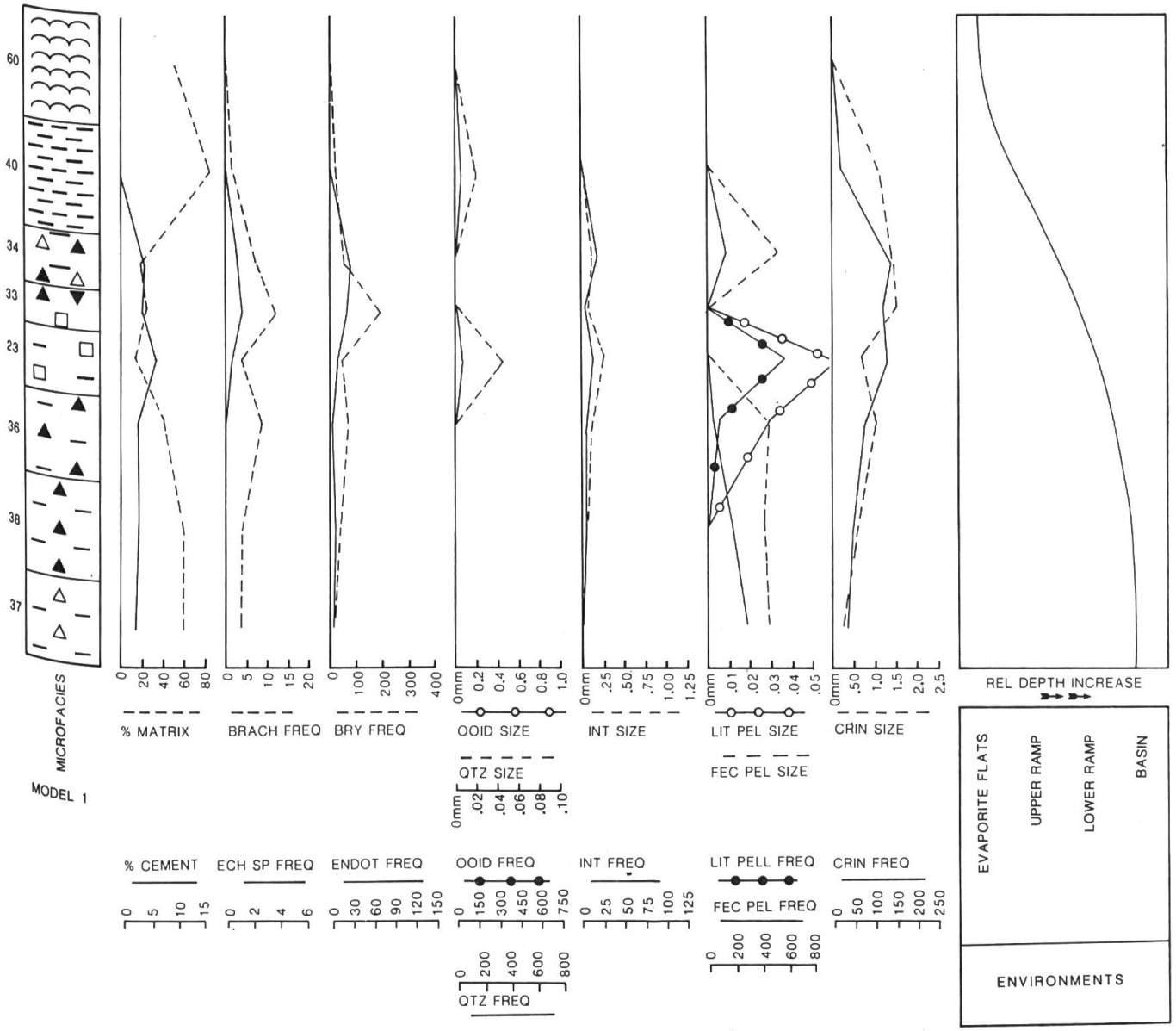

FIG. 5. — Ideal shallowing-up sequence for model 1.

favorable growth, which will subsequently evolve into a bioclastic bar, the crinoids decrease in importance both seaward and landward. Distribution of crinoids by currents was more towards the basin than towards the upper ramp, probably as an effect of the baffle zone created by the crinoids themselves in association with bryozoans and brachiopods. As early as this stage, the crinoid-bryozoan brachiopod baffle community affects to a large extent the distribution of all the biogenic and inorganic components, the matrix, and the cement.

Lithic Pellets, Fecal Pellets, and Intraclasts

The peaks of frequency and size of lithic pellets and intraclasts are both centered on the moderate energy lower ramp environment in association with the baffling

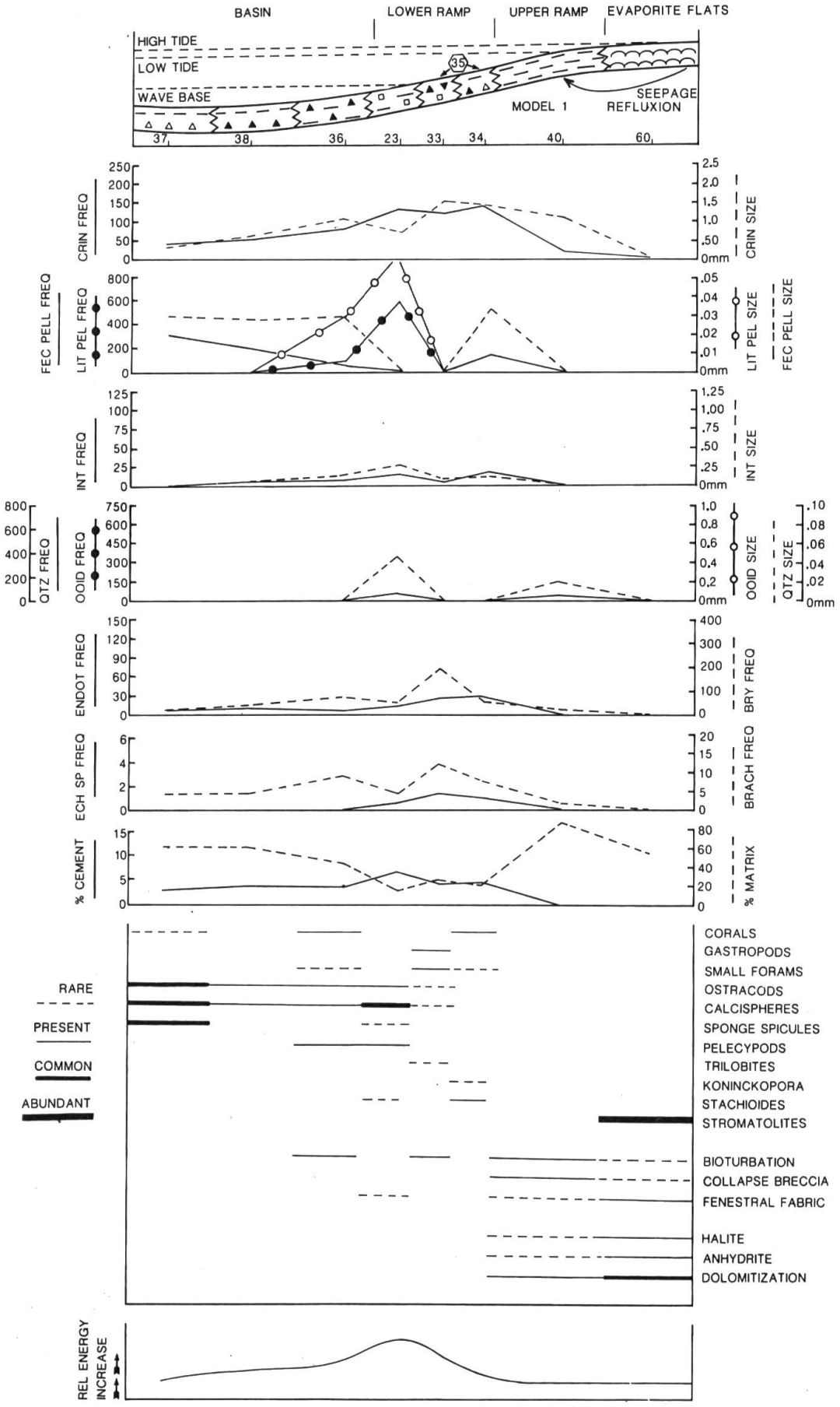

FIG. 6. — Horizontal depositional model 1.

crinoid-bryozoan-brachiopod community and indicate active intraformational reworking of the sediments in that particular zone with the intraclasts generation extending further into the upper ramp. Fecal pellet distribution corresponds to lower energy conditions both in basinal and protected upper ramp environments which are more amenable to extensive biogenic activity and preservation of fecal pellets. The greatest frequency of fecal pellets is in the basinal environment.

Detrital Quartz

The frequency and clasticity curves of quartz show peaks in two environments: at the foot of the lower ramp (average grain size of 0.05 mm) and in the upper ramp calcisiltites (average grain size of 0.02 mm). The upper ramp fine-grained quartz appears land derived and wind blown in contrast to the former coarse-grained quartz which probably was transported by rivers into the basin, distributed laterally by currents, and eventually trapped in the crinoidal baffle zone of the lower ramp.

Bryozoans, Brachiopods, and Echinoid Spines

They show maximum frequencies in the lower ramp and their distribution curves are slightly offset upslope from that of crinoids indicating that these organisms lived behind the protection of the crinoid baffle systems and participated significantly in constructing the incipient bioclastic bar. Bryozoans were probably among the early colonizers of the substratum along with the crinoids. The incipient bioclastic bar developed probably from microfacies 23 at the foot of the lower ramp which was the basinward edge of the crinoidal baffle zone. Another smaller peak of frequency of brachiopods and bryozoans is located basinward of the lower ramp baffle zone and fragments were dispersed and transported basinward by currents, hence the decreasing frequency from the edge of the lower ramp into the basin.

Endothyrids

Endothyra are ubiquitous, of low frequency, and extend from the open marine basinal environment to the upper ramp environment with concentration in the lower ramp.

Sparite Cement and Micrite Matrix

There is an inverse relationship for these two components. Cement has its peak frequency at the foot of the lower ramp (microfacies 23) in coincidence with wave base; it decreases asymmetrically landward and seaward but matrix increases asymmetrically away from the incipient bioclastic bar (microfacies 23, 33, and 34). There is more matrix on the upper ramp than in the basin because of the lower energy of currents in the upper ramp, a consequence of the baffling effect of the crinoidal buildups of the lower ramp. There is more cement in the basinal microfacies than in the upper ramp microfacies because of more current winnowing out of micritic matrix in the basinal environment. The relative energy curve for the en-

vironments is derived from the cement/matrix ratios as well as from grain sizes, rounding and sorting in the various microfacies.

Minor Components and Textural Features

Ostracods, calcispheres, and sponge spicules are common in the basinal environment with an apparent trapping of calcispheres in the crinoidal baffle zone of the lower ramp. All minor biogenic components essentially disappear in the upper ramp expressing the previously discussed restricted hypersaline conditions shown also by the presence of dolomitization, anhydrite, 'ghosts' of halite hopper crystals, collapse brecciation, bioturbation, and fenestral porosity. Algal mats are common in the evaporitic flats.

Depositional model 2

In depositional model 2 (Figures 7 and 8), a subtidal to low intertidal crinoidal-bryozoan bioclastic bar has developed separating a lagoonal environment from slope and basinal conditions. The bioclastic bar is represented by fairly well sorted, usually coarse sparite cemented to pressure-welded biocalcarenite that is often pelletoidal (microfacies, 31 and 32, 21, and 22). The lagoon is characterized by bioaccumulated brachiopod-bryozoan limestone (microfacies 35), biocalcarenite or intraclastic biocalcarenite with calcisiltite to bioclastic matrix (microfacies 34, 33, and 23), calcisiltite with rare bioclasts (microfacies 40). The evaporitic flat is represented by the stromatolites of microfacies 60. Compared to model 1, the extension of the evaporite flat is appreciably reduced and therefore the related dolomitization by seepage refluxion becomes a moderately active process. The slope is represented by biocalcarenite with bioclastic to calcisiltitic matrix (microfacies 33 and 34) and the basin shows mud-supported biocalcarenite (microfacies 36) and bioclastic, pelletoidal calcisiltite (microfacies 38 and 37).

Component Variations

Crinoids

Crinoid frequency and clasticity curves reach their peaks in coincidence with the bioclastic bar. The crinoids throve in the shallow water, moderate to high energy environment of the bioclastic bar, which corresponds to the peak energy of this model. The basinward and landward decrease of the frequency and clasticity of crinoids is due to transport of broken fragments away from the bioclastic bar. As in the previous model, the behavior of the crinoids affects to a large extent the position of the peaks of frequency and clasticity of other components.

Lithic Pellets, Fecal Pellets, and Intraclasts

Intraclasts have their peaks of frequency and clasticity in the bioclastic bar in coincidence with the crinoids while lithic pellets reach their peak for both frequency and clasticity behind the bioclastic bar as a result of abrasion because of slight

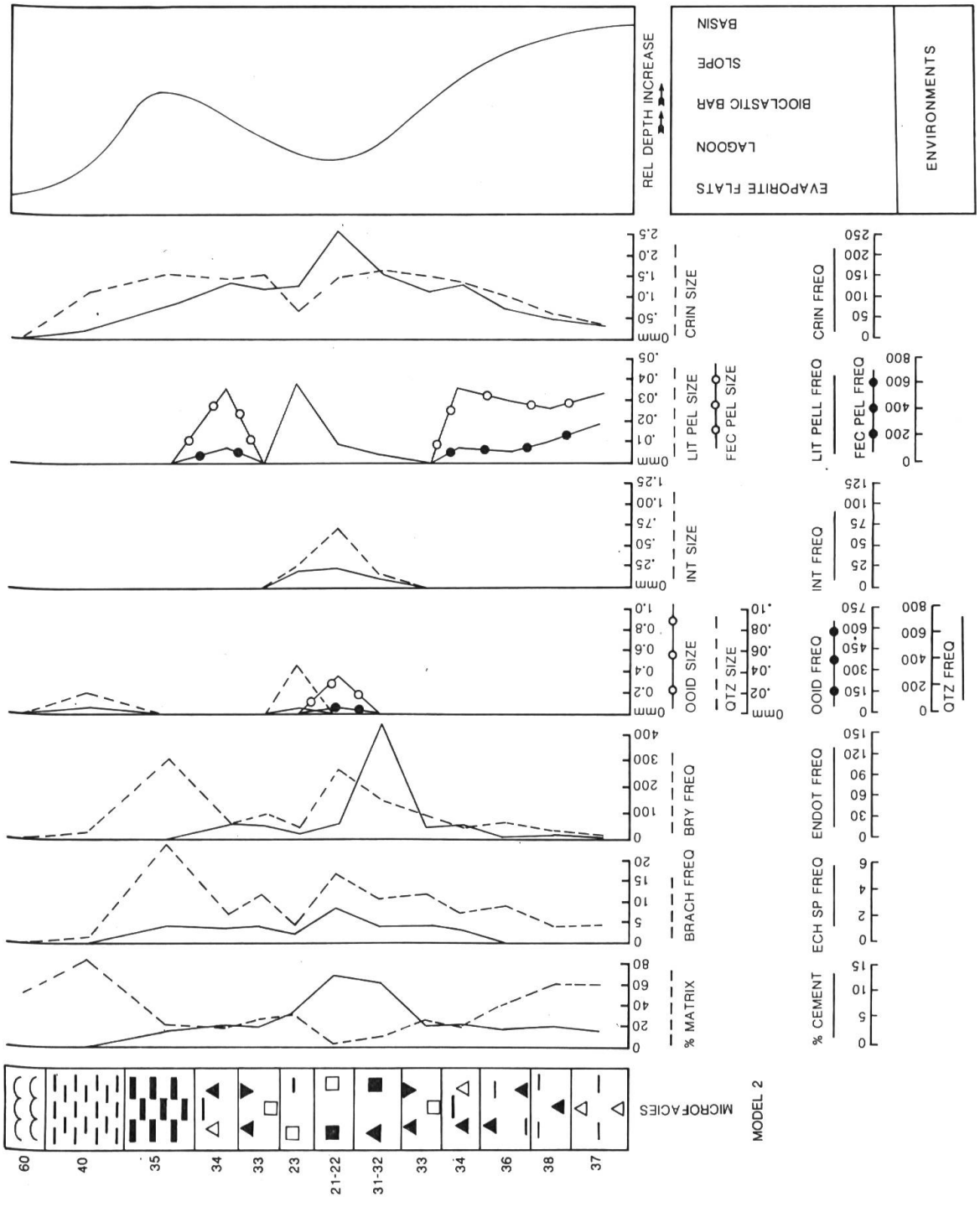

FIG. 7. — Ideal shallowing-up sequence for model 2.

lagoonward transport. The generation of intraclasts confirms the location of the maximum energy at the crinoidal bar. Fecal pellets have their frequency peak in the basin and decrease rapidly up the slope and towards the bioclastic bar. Another occurrence of fecal pellets is located in the lagoon. The fecal pellets are thus abundant

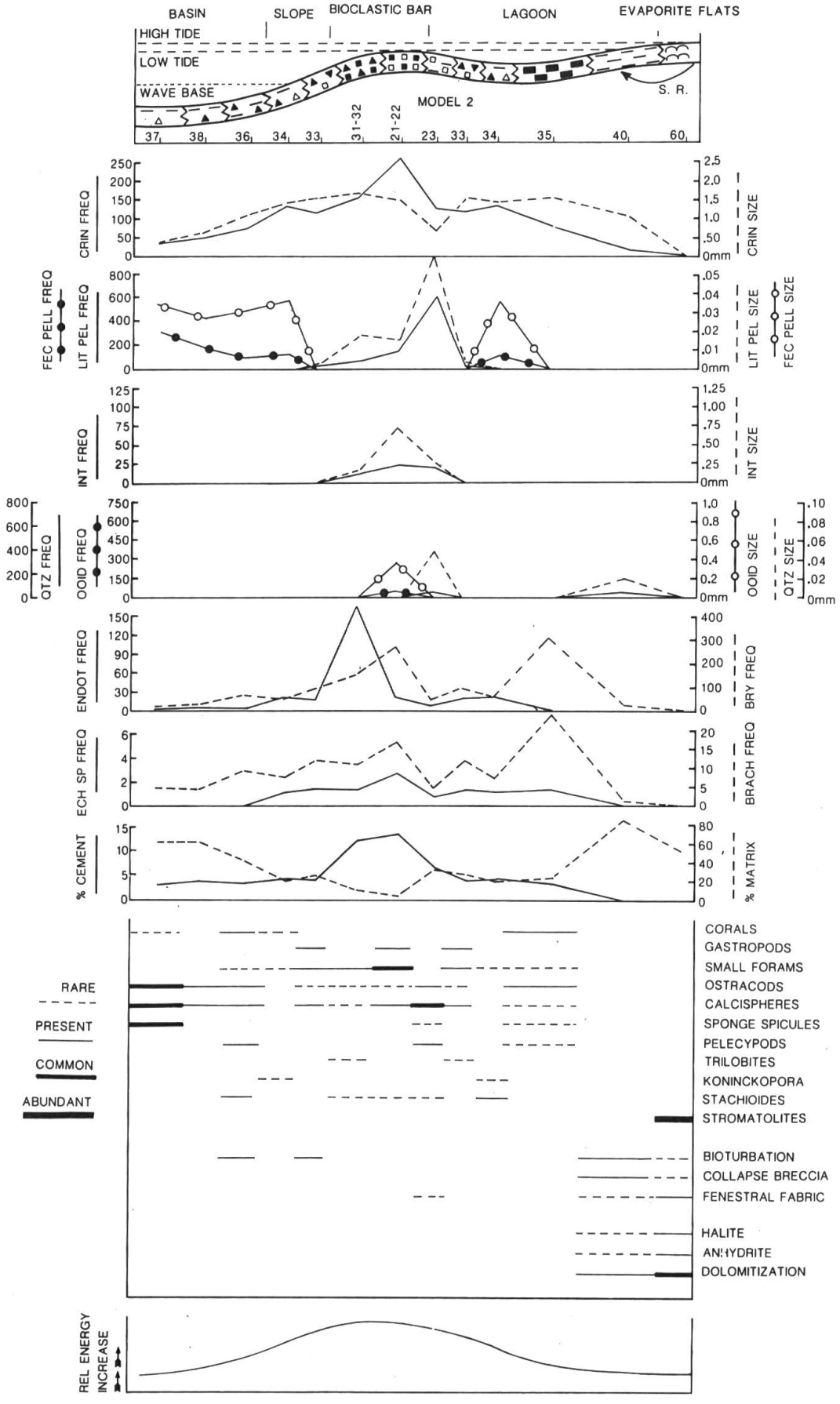

FIG. 8. — Horizontal depositional model 2.

in low energy environments where extensive infaunal activity can occur and have its products preserved.

Detrital Quartz

Fine sand-size quartz (0.02 mm), probably eolian in origin, occurs at the edge of the evaporite flats in contrast to coarser quartz (0.05 mm), probably fluvial, which with subsequent transport by marine currents occurs behind the bioclastic bar in coincidence with the concentration of lithic pellets.

Ooids

There is a minor occurrence of ooids in the bioclastic bar together with the peak of crinoid and intraclast production which indicates that locally, calcium carbonate saturation existed and allowed oolitization processes. This forecasts the evolution of the bioclastic bar into the oolitic bar-to-bank environment characterizing model 3.

Bryozoans, Brachiopods, and Echinoid Spines

Bryozoans and brachiopods frequency curves have a parallel behavior. A first peak is in the bioclastic bar indicating a community closely associated with crinoids and high energy conditions. Bioclasts of this community are transported basinward. A second peak is located in the lagoon which represents a community living in much lower energy. Preservation is enhanced and fragments tend to be larger.

The frequency curve of echinoid spines follows closely that of crinoids but with lower frequencies. Habitat and distribution process are the same.

Endothyrids

There is a peak of *Endothyra* frequency in the front of the bioclastic bar and a rapid decrease in both directions away from the bioclastic bar. Some *Endothyra* appear reworked and were transported across the bar into the lagoon.

Sparite Cement and Micrite Matrix

Cement is common in the bioclastic bar expressing the site of maximum energy of the model and decreases in both directions away from it. The micritic matrix has a peak in the basin, decreases towards the bioclastic bar where it reaches a minimum, then increases towards the lagoon which corresponds to its maximum development. The relative energy curve is derived in large part from the cement and matrix data.

Minor Components and Textural Features

Ostracods, calcispheres, and sponge spicules are common in the basin and, as the other biogenic components, they are distributed across the bioclastic bar into the lagoon indicating that the latter was in easy communication with open sea conditions. Small foraminifers are concentrated in the bioclastic bar and as in

model 1, calcispheres appear again trapped behind the bar by the baffling effect of crinoids and bryozoans. The landward side of the lagoon lacks bioclasts and is little bioturbated. This, in relation with the appearance of anhydrite, halite, and dolomitization, indicates a moderate influence of seepage refluxion brines.

Depositional model 3

Depositional model 3 represents the final stage of deposition in St. Louis time. The well developed bioclastic bar of model 2 has now evolved into a system of oolitic bars to banks (Figures 9 and 10). Model 3 consists of a narrow evaporitic flat of stromatolites (microfacies 60), a lagoon with slightly bioclastic calcisiltite (microfacies 40), grain-supported, often oolitic biocalcarenite with calcisiltite to

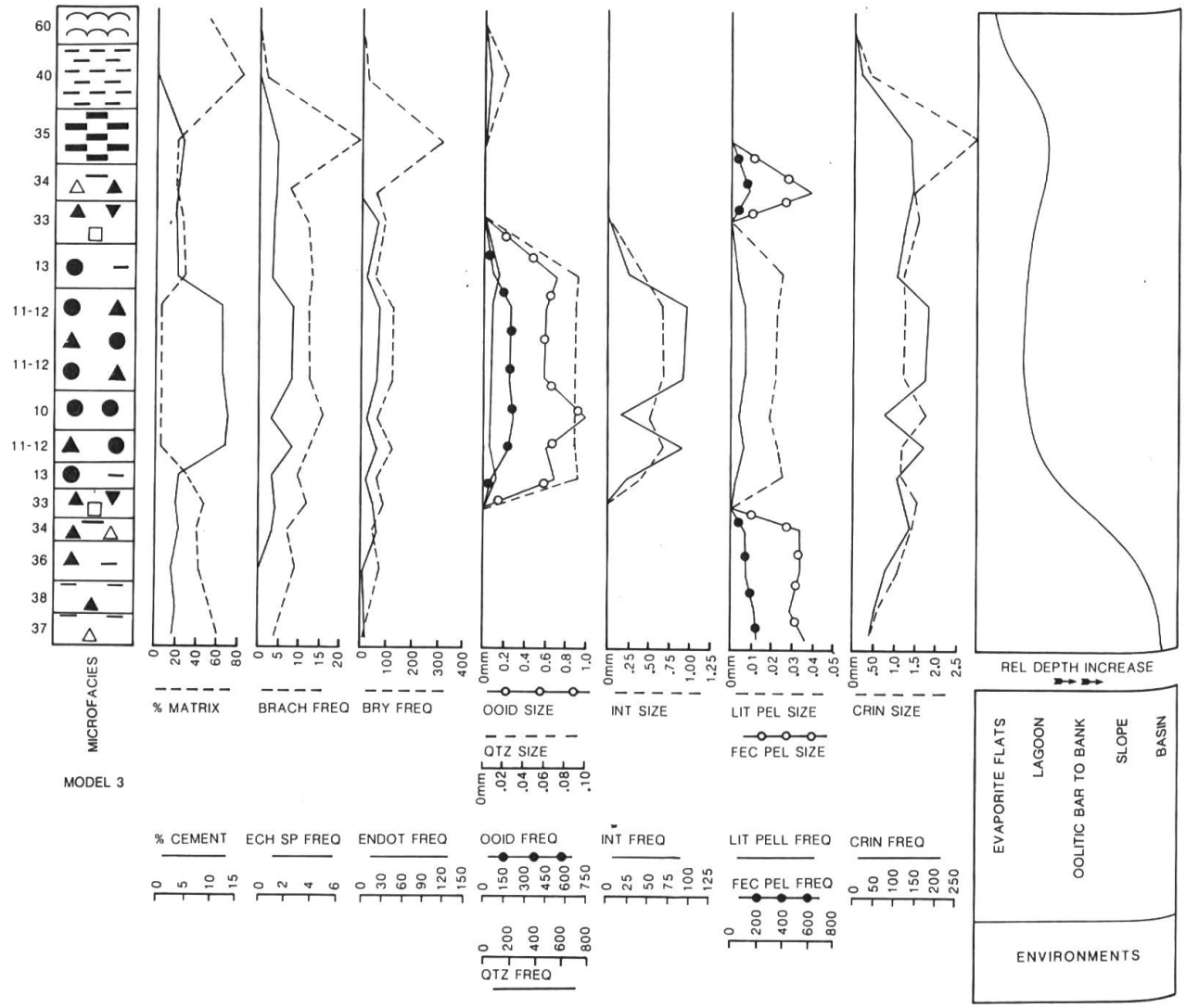

FIG. 9. — Ideal shallowing-up sequence for model 3.

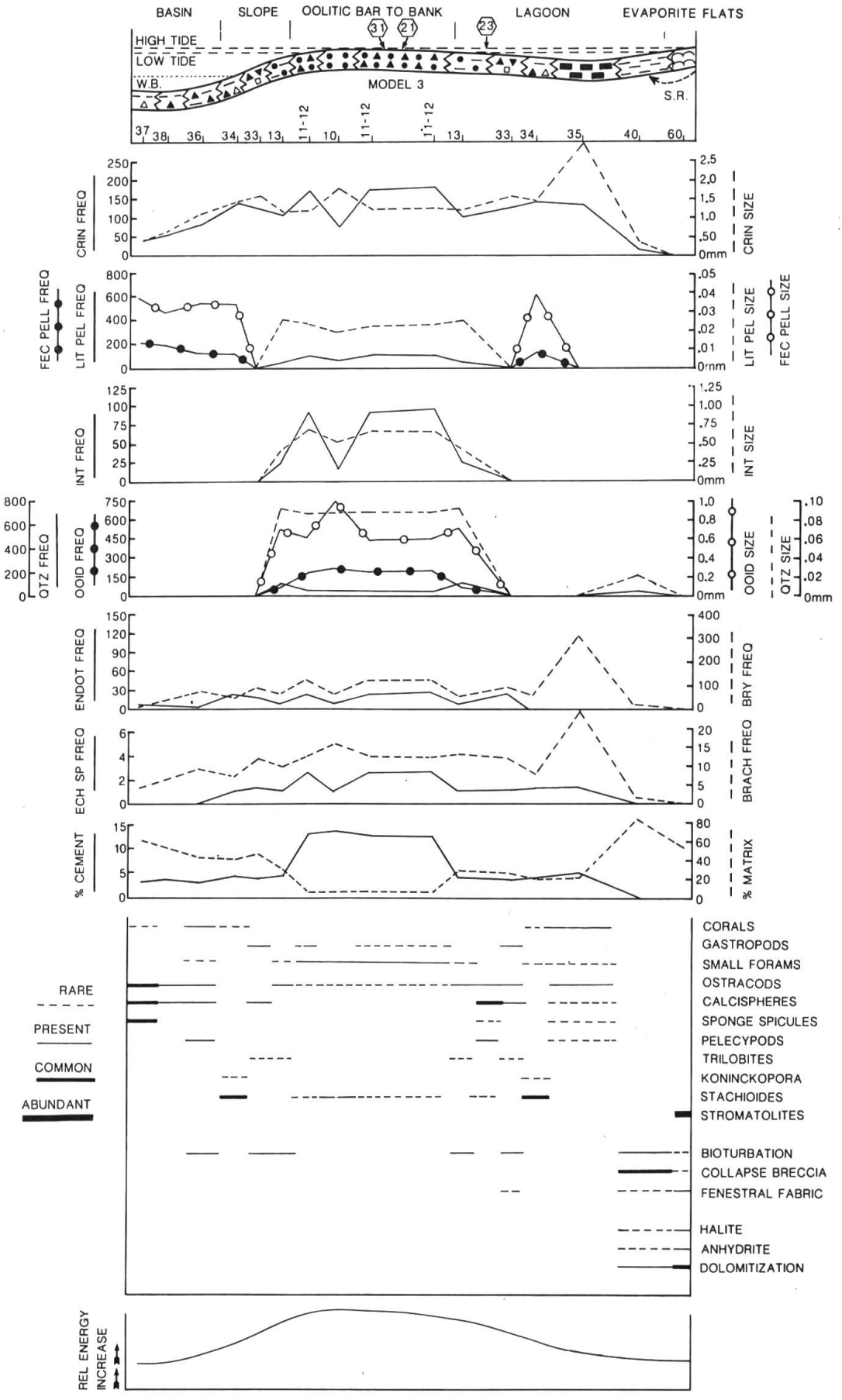

FIG. 10. — Horizontal depositional model 3.

bioclastic matrix (microfacies 33, 34, and 13), and bryozoan-brachiopod bioaccumulated limestone (microfacies 35). The latter is followed by an oolitic bar-to-bank environment with sparite cemented, often pressure-welded oolitic biocalcarenite (microfacies 10, 11, and 12), a slope environment with grain-supported, sometimes oolitic biocalcarenite with bioclastic to calcisiltitic matrix (microfacies 13, 33, and 34), and a basinal environment consisting of a mud-supported biocalcarenite (microfacies 36) and pelletoidal bituminous bioclastic calcisiltite (microfacies 38, 37).

Compared to model 2, the extension of the evaporitic flat is further reduced and therefore the related dolomitization by seepage refluxion becomes a minor process.

Component Variations

Crinoids

They are the major contributors to the bar-bank system. The widespread distribution of crinoids expresses the high energy conditions under which the bar-bank system developed. Crinoids were mechanically distributed basinwards from the bar-bank area and a second population of larger (average size of over 3 mm) crinoids occurs in the lagoon associated with peaks of frequency of bryozoans and brachiopods. As in the previous models, the position of the oolitic-crinoidal bar-to-bank system affects the distribution of almost all components.

Lithic Pellets, Fecal Pellets, and Intraclasts

Both lithic pellets and intraclasts are most abundant in the oolitic bar to bank environment indicating active intraformational reworking and distribution. As previously, fecal pellets have two peaks of abundance, first in the basin with decrease to zero as one progresses up the slope towards the bar-to-bank environment and, second, in the lagoon. Both fecal pellet peaks occur under conditions of low energy with active infauna and good preservation of the pellets.

Detrital Quartz

Fine sand-size detrital quartz (larger than 0.05 mm) occurs throughout the oolitic bar-to-bank as individual grains on either edges of the bank proper in the least oolitic bank microfacies (13), and as superficial ooid or ooid cores in the other bank microfacies (12, 11, and 10). On the landward edge of the lagoon are small occurrences of wind blown fine-grained (less than 0.02 mm) quartz.

Ooids

Ooids are a major component of the bank environment with corresponding maxima of their frequency and clasticity. Clasticity is highest near the frontal area of the bar-to-bank environments where maximum energy would be expected as well as best conditions for oolitization associated with currents rising up the slope.

Bryozoan, Brachiopods, and Echinoid Spines

Frequency curves of bryozoans and brachiopods are roughly parallel. A broad peak centers on the oolitic bar-to-bank suggesting a distinct population living in high energy conditions, but partially dispersed by currents. A second but narrower peak of higher frequency indicates another population living in the quieter lagoon which was apparently still well connected with open sea conditions. The frequency curve of echinoid spines follows that of crinoids forming a broad band that rises gently from the slope through the bar-to-bank and similarly decreases into the lagoon. The distribution of echinoid spines is regulated by the same factor as crinoids.

Endothyrids

Endothyra are ubiquitous from the basin through the slope, the bar and into the lagoon occurring as individual bioclasts or as ooid cores in the bar-to-bank environment.

Sparite Cement and Micrite Matrix

The two curves behave in an opposite manner. Cement is most abundant in the frontal area of the bar-to-bank in agreement with the highest energy of oolitization. It decreases in both directions while abundant matrix characterizes the low energy slope to basin environment on one side of the bar-to-bank and the low energy lagoonal environment on the other side where matrix abundance is greater than in the basin as a result of the protection afforded by the bar-to-bank. The relative energy curve for environments is derived to a large extent from the cement/matrix ratios.

Minor Components and Textural Features

Calcispheres, ostracods and sponge spicules are concentrated in the basinal microfacies. The oolitic bar-to-bank and the lagoon show a well developed suite of bioclasts with a concentration of calcispheres on the external shore of the lagoon. As soon as the influence of the seepage refluxion is felt (halite, anhydrite, dolomitization), fossils virtually disappear and only stromatolites characterize the supratidal environment.

STRATIGRAPHIC SECTIONS AND VERTICAL SUCCESSION OF MICROFACIES

The petrographic data derived from the study of the thin sections were plotted for all stratigraphic sections (Diaby, 1984). The section of the Caldwell County core (Figure 3) is a perfect example of vertical superposition of deposits of the three depositional models and can be used to introduce the type of graphic representation used in this work (Figures 11 and 12). The latter is as follows from left to right:

1) Column of microfacies identified in the sections with control points and depths for the cores and distance above base for the field sections in feet.

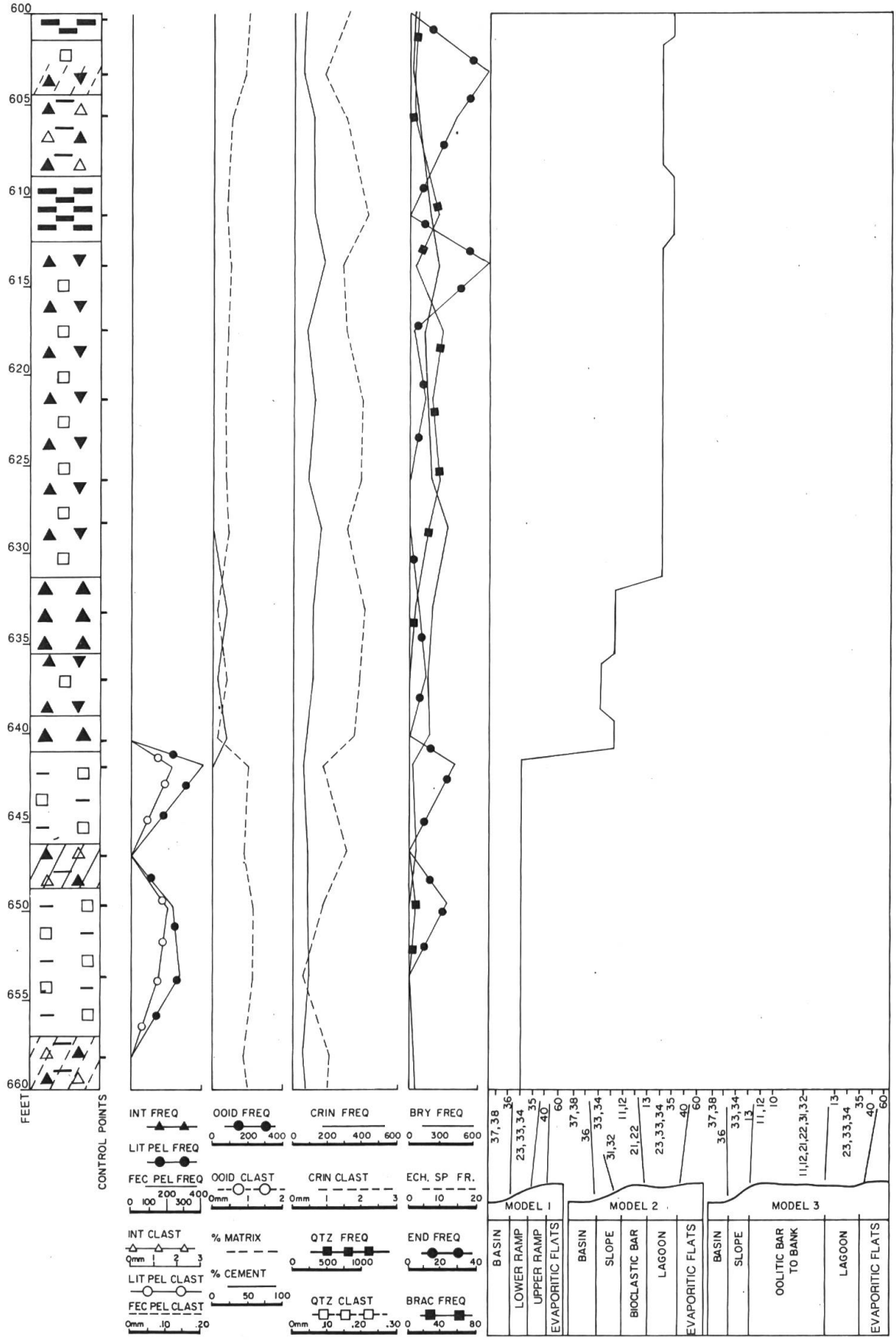

FIG. 11. — Caldwell County core, Kentucky (600′ to 660′).

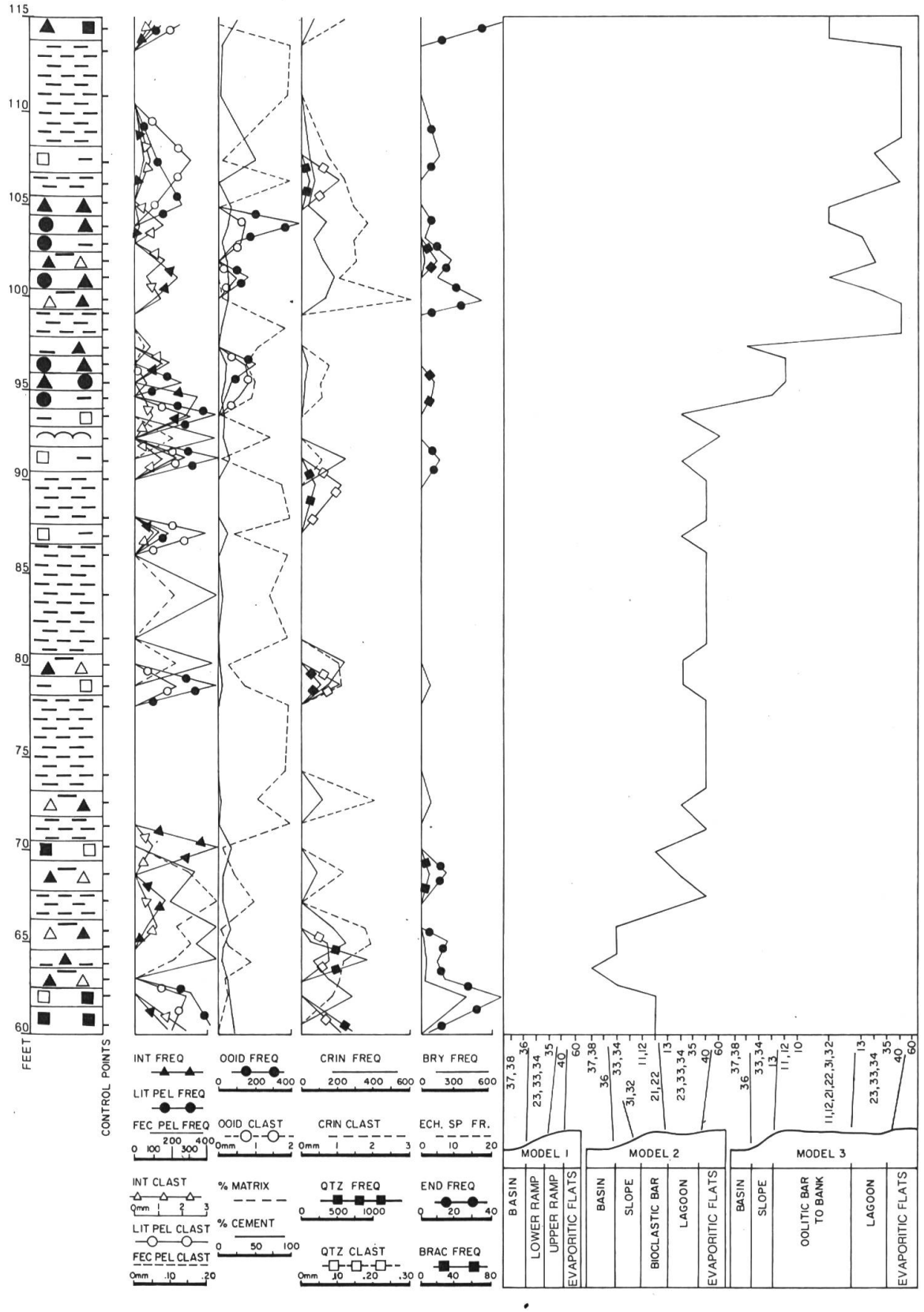

FIG. 12. — Olin quarry, Alton, Illinois (60′ to 115′).

2) Set of four vertical curves showing clasticity and frequency for selected components as well as percent cement and percent matrix for the whole rock.

3) On the right, a simplified sketch of the three depositional models is used as horizontal scale for the curve of evolution of the environments through time. Models 1, 2, and 3 are juxtaposed from left to right. All three share the microfacies of depositional model 1 (microfacies 60, 40, 34, 35, 33, 23, 36, 38, and 37). The environmental variation curve is moved from model 1 to mode 2 (Figure 11) when the sparite cemented biocalcarenites to pelletoidal biocalcarenites (microfacies 32, 22, 31, and 21), characteristic of the bioclastic bar of model 2 are encountered in the sections or cores. Likewise, the environmental variation curve is moved from model 2 to model 3 (Figure 12) when the grain-supported to pressure welded oolitic biocalcarenites (microfacies 10, 11, and 12) of the oolitic bar-to-bank of model 3 appear in the sections.

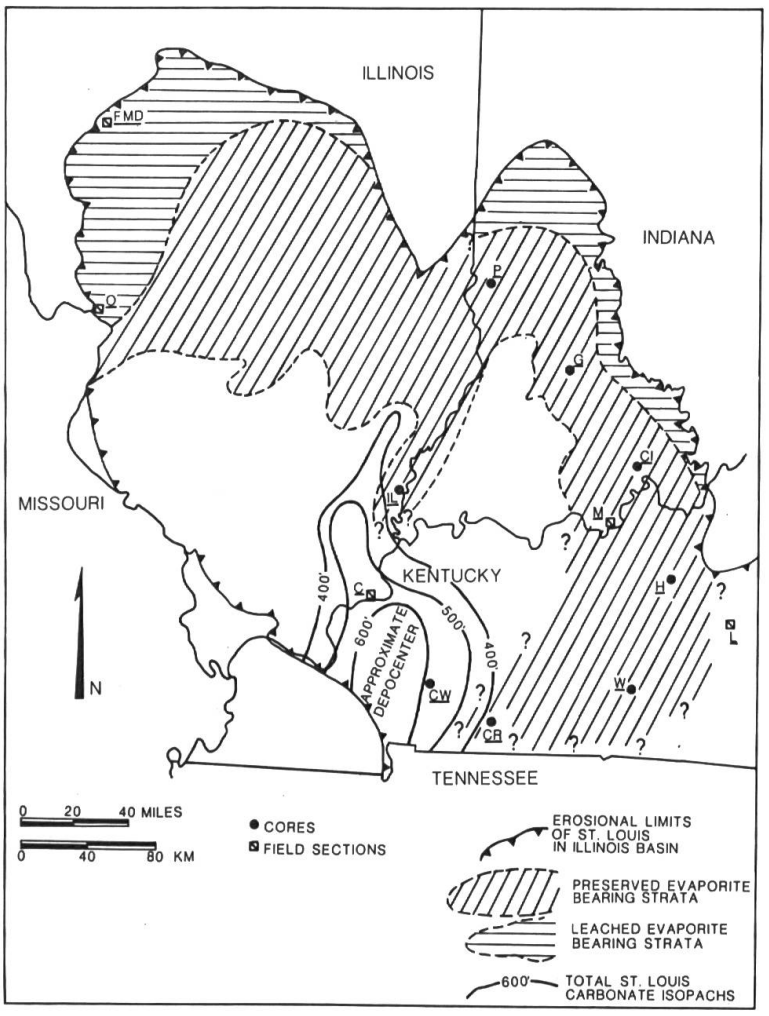

FIG. 13. — St. Louis lithofacies and location map of sections.

BASINWIDE EVOLUTION OF ST. LOUIS LIMESTONE

Vertical succession of depositional models

The St. Louis Limestone in the Illinois Basin (Figure 13) represents a vast embayment open to the south with a present-day northern erosional limit beneath the Pennsylvanian and a portion of the depocenter detectable in southwest Illinois (Gallatin, Hamilton, Hardin, Pope, Saline, and White Counties) and in western Kentucky (Caldwell, Crittenden, Trigg, and Lyon Counties). The distribution of the evaporite-bearing zone of the lower part of the St. Louis corresponding to depositional model 1, indicates the great extent during that particular time interval of the supratidal evaporitic flats (coastal sabkha) grading basinward into a carbonate ramp.

A simplified basin cross-section of the St. Louis Limestone oriented SW-NE was prepared from the following cores: Crawford County, Indiana, Warren County, Kentucky, Christian County, Kentucky, and Caldwell County, Kentucky (Figure 14) in order to show the time and space relationships of the three depositional models from basin margins in the NE to the depocenter in the SW.

Environmental variation curves representing the interpretation of the microfacies were plotted in each vertical section and correlated across the basin using their breaks (changes of depositional model), thus revealing the limits of the three successive depositional models. The Crawford County, Indiana, core is on the margin of the basin and shows only model 1 deposits throughout St. Louis time. The Warren County, Kentucky, core further from the basin margin, shows depositional model 1 microfacies over most of its length except for the top third where microfacies representing depositional model 2 are encountered. More towards the center of the basin, the Christian County, Kentucky, core shows a superposition of deposits from models 1, 2, and 3. Finally, very near the depocenter, the Caldwell County, Kentucky, core shows an ideal succession with full development of deposits from models 1, 2, and 3.

The shape of the limits of the successive depositional models clearly reveals how, starting from a former depositional surface corresponding to the terminal progradation of the Salem Limestone, the geometry of the initial ramp model of the St. Louis Limestone evolved into the bioclastic bar of model 2 and eventually into a fully developed oolitic bar-to-bank carbonate platform. This morphological evolution corresponds to a rapid progradation of medium to high energy carbonates which terminates St. Louis time deposition. Meanwhile, along the margins, a zone of low energy carbonates persisted whereas a supratidal flat area gradually decreased in importance.

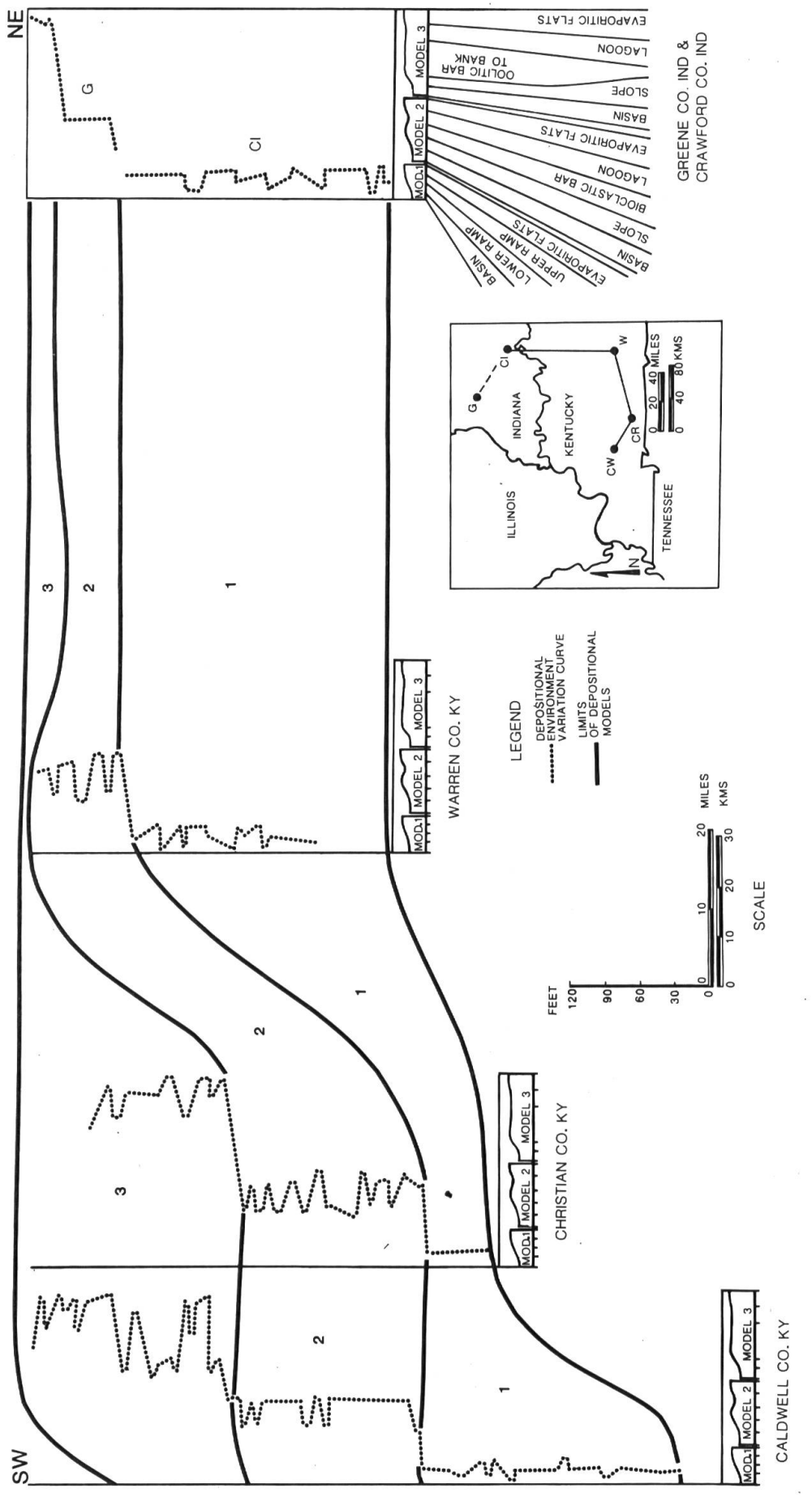

FIG. 14. — Cross-section with basinwide evolution in time of St. Louis Limestone from ramp to bar to platform.

Comparison with similar depositional models

A comparison between the succession of three depositional models of the St. Louis and published examples (see Carozzi, 1983) reveals interesting similarities and differences.

For instance, depositional model 1, a carbonate ramp as proposed by Ahr (1973) has great similarities with the ramp models proposed for the Bird Spring Group, Pennsylvanian of Nevada (Heath, Lumsden, and Carozzi, 1967), for the Platteville Group, Middle Ordovician of Illinois (Kuhnhenn and Carozzi, 1977), and particularly for the Smackover Limestone, Upper Jurassic of Texas (Budd and Loucks, 1981) which terminates landwards into a well developed sabkha environment.

Depositional model 2 characterized by its subtidal bioclastic bar controlled by crinoids is similar in many aspects to the models proposed for the Pogonip Group, Middle Ordovician of Arrow Canyon, Nevada (Stricker and Carozzi, 1973), the Rundle Group, Mississippian, Alberta, Canada (Walpole and Carozzi, 1961), the Kinkaid Formation, Upper Mississippian, Illinois Basin (Lasemi and Carozzi, 1981) and the Upper Bird Spring Group, Upper Pennsylvanian-Lower Permian (Nowak and Carozzi, 1972).

Depositional model 3, an oolitic bar-to-bank platform is similar to the model proposed for the Ste. Genevieve Limestone, Middle Mississippian (Rao and Carozzi, 1971).

Whereas all the above-cited depositional models have lasted for appreciable lengths of geological time, a unique feature of St. Louis deposition is the rapid succession (lasting only through two conodont zones) of its three models.

DIAGENESIS

The diagenetic features observed in the St. Louis Limestone (Figure 15) are complex, but can be interpreted as representing depositional and post-depositional changes that took place in the following environments: 1) marine phreatic, 2) marine vadose, 3) undersaturated freshwater phreatic, 4) saturated freshwater phreatic, 5) mixing marine freshwater phreatic, and 6) burial. The diagenetic features observed will be described and interpreted in the above mentioned order of environments.

Marine phreatic environment

Micritization of all bioclasts (Plate 2, E) is widespread and caused by action of endolithic algae. Fairly thick micritic envelopes are often generated. Intraclasts consisting of calcisiltite to bioclastic calcisiltite occur in the high energy sparite cemented biocalcarenites (microfacies 21 and 22). They show early submarine

DIAGENETIC ENVIRONMENTS / DIAGENETIC FEATURES	MARINE PHREATIC	MARINE VADOSE (SABKHA BRINES)	UNDERSATURATED FRESHWATER PHREATIC	SATURATED FRESHWATER PHREATIC	MIXING MARINE FRESHWATER PHREATIC	BURIAL
MICRITIZATION	—					
INTRACLAST CEMENTATION OXIDATION & REWORKING	—					
EARLY COMPACTION (I) (PRESSURE-SOLUTION)	—					
THIN ISOPACHOUS RIM CEMENT	—					
EARLY COMPACTION (II)	—					
GEOPETAL ORGANIZATION OF INTERNAL SEDIMENT	—					
PERVASIVE DOLOMITIZATION		—				
ANHYDRITIZATION (I) EUHEDRAL CRYSTALS & NODULES IN MICRITE		—				
LEACHING OF ARAGONITIC SHELLS & DISSOLUTION OF EVAPORITES & DOLOMITE			—			
EARLY FRACTURATION			—			
FRACTURE FILLING CALCITE				—		
CALCITIZATION OF EUHEDRAL ANHYDRITE				—		
SYNTAXIAL RIM CEMENT				—		
SPARITE MOSAIC CEMENT				—		
NEOMORPHISM (STABILIZATION OF RIM CEMENT)				—		
PERVASIVE SILICIFICATION					—	
LATE COMPACTION (STYLOLITES)						—
BURIAL DISSOLUTION OF CALCITE, DOLOMITE? ANHYDRITE?						—
ANHYDRITE (II) REPLACEMENT OF BIOCLASTS, OOIDS & SPARITE CEMENT						—
LATE BURIAL FRACTURATION						—
LATE FRACTURE FILLING CALCITE CEMENT						—
BLADED ANHYDRITE (III) REPLACING LATE FRACTURE FILLING CALCITE						—
LATE DOLOMITIZATION (SADDLE DOLOMITE)						—
	➤	➤	➤ TIME	➤	➤	➤

FIG. 15. — Diagenetic features and environments.

lithification followed by reworking and abrasion under agitated conditions. Some intraclasts are often slightly oxidized on their margins.

Early compaction I is expressed by pressure-solution and reciprocal deformation of bioclasts, deformation at ooid contacts, minor spalling of outer cortical layers, and formation of chain ooids. The early nature of this episode of compaction is demonstrated by the absence of submarine rim cement between deformed components.

Precipitation of fibrous thin isopachous rims around ooids and crinoids characterizes the well sorted grain-supported sparite cemented oolitic biocalcarenites (Plate 2, F). The fibrous nature of the isopachous rim cement indicates a probably high-Mg calcite composition later stabilized in the freshwater phreatic environment.

Early compaction II follows precipitation of the isopachous rim cement. The latter shows partial dissolution at contact of ooids as well as cases of reciprocal interpenetration of two ooids with isopachous rim cement and minor spalling (Plate 2, G).

Geopetal pelletoidal internal sediment infills the interooid cavities, overlies the isopachous fibrous rim cement, and is in turn overlain by freshwater phreatic calcite cement which fills the remainder of the intergranular voids (Plate 2, F, G; Plate, 3, A).

Marine vadose environment

Pervasive dolomitization takes place in the calcisiltites (microfacies 40) of the upper ramp (model 1) or edge of the lagoon (models 1 and 2). The dolomite occurs as scattered rhombs (25 to 40 microns) representing 50 to 60% of the rock. The supersaturated brines are derived from high evaporation in the supratidal evaporite flats (sabkha environment); they migrated by seepage refluxion (Adams and Rhodes, 1960) toward the calcisiltites of the upper ramp or edge of the lagoon where dolimitization took place. This transitional (sabkha to non-sabkha) environment is very similar to the one postulated by Shukla and Friedman (1983) for the Lockport Formation because it lacks most of the sabkha associated features but shows dolomitization and anhydritization. In the present case, minor stromatolites were observed and corroborated the near-sabkha location.

In association with the pervasive dolomitization, small scattered euhedral anhydrite crystals (anhydrite I) also form from the sabkha-derived brines (Plate 2, H). Locally, when permeability conditions allow, the anhydrite crystals can grow fairly large (3 mm or even larger). Small scattered nodules or small poorly formed rosette structures may occur.

Undersaturated freshwater phreatic environment

In this diagenetic environment, leaching of thus far preserved aragonitic or high-Mg calcitic shells takes place (Longman, 1980). Micritized molds of molluscan shells are subsequently infilled with bladed to mosaic sparite cement. Some dissolution

of anhydrite crystals and of small dolomite rhombs may also occur, creating crystal moldic porosity. Very characteristic are subparallel early fractures perpendicular to bedding, which cut across the ooids, the fibrous rim cement, and the geopetal internal sediment. The fractures are filled with calcite cement which is in optical continuity with the cavity filling cement only at the extremities of the fractures and when the latter are wide (Plate 3, A).

The above criteria indicate that this early fracturation phase occurred in the undersaturated freshwater phreatic environment. Then, either late in that environment or very early in the saturated freshwater phreatic environment (before most of the cavity filling sparite cement formed), the fractures were infilled with calcite cement. Fracturation is probably due to dissolution of subjacent evaporites with consequent partial 'collapse' of the oolitic biocalcarenite. This early fracturation and cementation phase is to be distinguished from the later (burial) fracturation and cementation.

Saturated freshwater phreatic environment

In this diagenetic environment, partial to complete pseudomorphic calcitization of euhedral anhydrite takes place (Plate 2, H). Disseminated small dolomite rhombs from the marine vadose pervasive dolomitization phase may remain unaffected. The most common process is the formation of clear syntaxial calcite overgrowths on the nonmicritized crinoidal bioclasts which engulf the other constituents. The syntaxial overgrowths are juxtaposed with intergranular cavity filling sparite mosaic (Plate 3, B). The latter, at places, grades into fracture filling (early fracturation phase) microcrystalline calcite (Plate 3, A). In this diagenetic environment, neomorphism is widespread among gastropods and bioclasts of green algae (Dasyclads ?). An impure pseudomicrosparite is a typical product of this process in the latter.

Mixing marine freshwater phreatic environment

Silicification occurs as euhedral quartz crystals replacing cores and outer cortical layers of ooids (Plate 3, C) and pervasive fibroradiated microcrystalline quartz occuring inside anhydrite nodules. This episode of silicification follows the freshwater phreatic cementation because cases exist where sparite cemented biocalcarenites (microfacies 32) are entirely silicified. The attribution of silicification to the mixing marine freshwater phreatic environment is based on the model presented by Knauth (1979).

Burial environment

Late compaction expressed by stylolites with thick insoluble residue occur both in pelletoidal biocalcarenites with calcisiltite matrix and in biocalcarenites, intersecting all constituents and cement.

Partial dissolution of cavity filling calcite cement occurs at this stage creating secondary porosity in the oolitic biocalcarenite (Plate 3, D). It is possible that in this environment, dolomite and anhydrite which may have survived the leaching of the undersaturated freshwater phreatic environment are eventually dissolved.

Pervasive anhydrite (anhydrite II) replacement of bioclasts, ooids, and sparite cement in the oolitic biocalcarenites by connate waters occurs also at this stage (Plate 3, E). The anhydrite is coarse, euhedral to subhedral, sometimes lath-shaped, and corresponds to the crystallotopic morphology described by Maiklem *et al.* (1969). When replacing cavity filling sparite cement, the anhydrite is often poikilotopic. The timing of this second phase of anhydritization is shown by the fact that it replaces silicified bryozoans (Plate 3, F). It is possible that the source of the anhydrite-rich burial fluids may be a recycling of the anhydrite of the lower part of the St. Louis (Figure 14).

Oolitic biocalcarenites display late burial fractures which cut across the partially anhydritized sparite cemented oolitic biocalcarenites of the previous diagenetic event and are filled by sparite calcite cement (Plate 3, G). This cement is in turn partially replaced by bladed anhydrite III (Plate 3, G).

In large fractures of some pelletoidal calcisiltites, late dolomitic cement with undulose extinction occurs (Plate 3, H). None of the samples on hand permitted exact determination of the relative timing of the saddle dolomitization with respect to the other burial events. The work of Radke and Mathis (1980), which indicates that saddle dolomite formed in the burial environment at temperatures of the order of 100 to 150 degrees C, would allow to consider it as one of the latest if not the last burial diagenesis event in the samples studied.

CONCLUSIONS

The 1542 oriented samples studied permitted recognition of 16 microfacies. Their vertical succession and correlation in the sections and cores, led to construction of three ideal shallowing upwards sequences which translated horizontally into three depositional models.

Model 1 consists of: large supratidal evaporitic flats, intertidal to subtidal upper ramp, subtidal lower ramp, and basinal environment. Model 2 shows moderate size supratidal evaporitic flats, lagoon, bioclastic bar, slope, and basinal environment. Model 3 has very narrow supratidal evaporitic flats, lagoon, wide oolitic bar-to-bank, slope, and basinal environment.

The three depositional models followed one another in time expressing a progradation of the medium to high energy carbonates towards the depocenter as a ramp baffle zone (model 1) to a bioclastic bar (model 2), and eventually to an oolitic bar-to-bank system (model 3).

Dolomitization by seepage refluxion of brines derived from the evaporitic flats is strong in the upper ramp calcisiltites of model 1, moderate in the lagoonal calcisiltites of model 2, and minimal in the lagoonal calcisiltites of model 3.

The samples studied show petrographic evidence of diagenesis in the following environments: 1) Marine phreatic (micritization, reworking, compaction, isopachous fibrous rim cement, internal sediment, and fracturation), 2) Marine vadose (pervasive dolomitization and anhydritization), 3) Undersaturated freshwater phreatic (leaching of aragonitic shells, dissolution of anhydrite, and dolomite), 4) Saturated freshwater phreatic (calcitization of anhydrite, syntaxial overgrowths, cavity filling calcite cement, and neomorphism), 5) Mixing marine freshwater phreatic (silicification), 6) Burial (compaction with stylolitization, partial dissolution of cavity filling cement, pervasive anhydritization, fracturation and fracture filling calcite, late fracture filling saddle dolomite).

LIST OF REFERENCES

ADAMS, J. E. and M. L. RHODES (1960). Dolomitization by seepage refluxion: *Am. Assoc. Petroleum Geologists Bull.*, v. 44, pp. 1912-1920.

AHR, W. M. (1973). The carbonate ramp: an alternative to the shelf model: *Trans. Gulf Coast Assoc. Geol. Soc.*, v. 23, pp. 221-225.

BAXTER, J. W. and P. L. BRENCKLE (1982). Preliminary statement on Mississippian calcareous foraminiferal succession of the Midcontinent (U.S.A.) and their correlation to western Europe: *Newsl. Strat.*, v. 11, pp. 136-153.

BUDD, D. A. and R. G. LOUCKS (1981). Smackover and Lower Buckner Formations, south Texas: Depositional systems on a Jurassic carbonate ramp: *Texas Bureau of Econ. Geol., Rept. Invest.* No. 112, 38 p.

CAROZZI, A. V. (1958). Micromechanisms of sedimentation in the epicontinental environment: *Jour. Sed. Petrology*, v. 28, pp. 133-150.

—— (1961). Reef petrography of the Beaverhill Lake Formation, Upper Devonian, Swan Hills area, Alberta, Canada: *Jour Sed. Petrology*, v. 31, pp. 497-513.

—— (1983). Modelos deposicionales carbonaticos: *Ass. Geologica Argentina, Ser. B, Didactica y Complementaria* No. 11, v. I, 111 p., v. II, 197 p.

CAROZZI, A. V. and I. DIABY (1981). Microfacies and depositional model of the Salem Limestone (Middle Mississippian), southwestern Illinois, U.S.A.: *VIII Congreso Geologico Argentino, San Luis, Actas*, v. II, pp. 435-457.

DEMIRMEN, F. (1969). Multivariate procedures and Fortran IV program for evaluation and improvement of classifications: *Kansas State Geol. Survey Computer Contr.* No. 31, 51 p.

DEVER, G. R. Jr. and P. MCGRAIN (1969). High-calcium and low-magnesium limestone resources in the region of the Lower Cumberland, Tennessee and Ohio valleys, Western Kentucky: *Kentucky Geol. Survey Bull.* No. 5, 192 p.

DIABY, I. (1984). Petrography, diagenesis and depositional models of the St. Louis Limestone, Valmeyeran (Middle Mississippian), Illinois Basin, U.S.A.: *Unpubl. Ph. D. thesis, Univ. of Illinois (Urbana-Champaign)*, 185 p.

FRENCH, R. R. and L. F. ROONEY (1969). Gypsum resources of Indiana: *Indiana Dept. Nat. Resources, Geol. Survey Bull.* 42-A, 34 p.

HEATH, C. P., D. N. LUMSDEN, and A. V. CAROZZI (1967). Petrography of a carbonate transgressive-regressive sequence: The Bird Spring Group (Pennsylvanian), Arrow Canyon Range, Clark County, Nevada: *Jour. Sed. Petrology*, v. 37, pp. 377-400.

KNAUTH, L. P. (1979). A model for the origin of chert in limestone: *Geology*, v. 7, pp. 274-277.

KREY, F. (1924). Structural reconnaissance of the Mississippi valley area from Old Monroe, Missouri to Nauvoo, Illinois: *Illinois State Geol. Survey Bull.* No. 45, 86 p.

KUHNHENN, G. L. and A. V. CAROZZI (1971). Carbonate microfacies of the Platteville Group (Middle Ordovician), Lee and Lasalle Counties, Illinois: *Archives Sciences Genève*, v. 30, pp. 179-212.

KRUMBEIN, W. C. (1951). Occurrence and lithologic associations of evaporites in the United States: *Jour. Sed. Petrology*, v. 21, pp. 63-81.

LASEMI, Y. and A. V. CAROZZI (1981). Carbonate microfacies and depositional environments of the Kinkaid Formation (Upper Mississippian) of the Illinois Basin, U.S.A.: *VIII Congreso Geologico Argentino, San Luis, Actas*, v. II, pp. 357-384.

LINEBACK, J. A. (1972). Lateral gradation of the Salem and St. Louis Limestones (Middle Mississippian) in Illinois: *Illinois State Geol. Survey. Circ.* 474, 32 p.

LONGMAN, M. W. (1980). Carbonate diagenetic textures from near-surface diagenetic environments: *Am. Assoc. Petroleum Geologists Bull.*, v. 64, pp. 461-487.

MAIKLEM, W. R., D. G. BEBOUT and R. P. GLAISTER (1969). Classification of anhydrite — A practical approach: *Canadian Petroleum Geologists Bull.*, v. 17, pp. 194-233.

MCGRAIN, P. and W. L. HELTON (1964). Gypsum and anhydrite in the St. Louis Limestone in Northwestern Kentucky: *Kentucky Geol. Survey Inf. Circ.* No. 13, 26 p.

MCGREGOR, D. J. (1954). Gypsum and anhydrite in southwestern Indiana: *Indiana State Geol. Survey Rept. of Progress* No. 8, 24 p.

MIDDLETON, G. V. (1973). Johannes Walther's Law of the correlation of facies: *Geol. Soc. America Bull.*, v. 84, pp. 979-988.

NOVAK, F. J. and A. V. CAROZZI (1973). Microfacies of the Upper Bird Spring Group (Pennsylvanian-Permian), Arrow Canyon Range, Clark County, Nevada: *Archives Sciences Genève*, v. 25, pp. 343-382.

PATTON, J. B. (1949). Crushed stone in Indiana: *Dept. of Conservation, Division of Geology, Rept of Progress* No. 3, 47 p.

PINSAK, A. P. (1957). Subsurface stratigraphy of the Salem Limestone and associated formations in Indiana: *Indiana State Geol. Survey Bull.* No. 11, 62 p.

RADKE, B. M. and R. L. MATHIS (1980). On the formation and occurrence of saddle dolomite: *Jour. Sed. Petrology*, v. 50, pp. 1149-1168.

RAO, C. P. and A. V. CAROZZI (1971). Application of computer techniques to the petrographic study of oolitic environments, Ste. Genevieve Limestone (Middle Mississippian), southern Illinois and eastern Missouri: *Archives Sciences Genève*, v. 24, pp. 17-55.

REXROAD, C. B. and C. COLLINSON (1963). Conodonts from the St. Louis Formation (Valmeyeran Series) of Illinois, Indiana and Missouri: *Illinois State Geol. Survey Circ.* No. 355, 28 p.

SAXBY, D. B. and J. E. LAMAR (1957). Gypsum and anhydrite in Illinois: *Illinois State Geol. Survey Circ.* No. 226, 26 p.

SHUKLA, V. and G. M. FRIEDMAN (1983). Dolomitization and diagenesis in a shallowing-upward sequence: the Lockport Formation (Middle Silurian), New York State: *Jour. Sed. Petrology*, v. 53, pp. 703-717.

SOUPAC (1976). Soupac program descriptions, University of Illinois, Urbana-Champaign: *C.S.O.*, v. 1.

STRICKER, G. D .and A. V. CAROZZI (1973). Carbonate microfacies of the Pogonip Group (Lower Ordovician), Arrow Canyon Range, Clark County, Nevada, U.S.A.: *Bull. Centre Rech. Pau-S.N.P.A.*, v. 7, pp. 499-541.

WALPOLE, R. L. and A. V. CAROZZI (1961). Microfacies study of the Rundle Group (Mississippian) of Front Ranges, Central Alberta, Canada: *Am. Assoc. Petroleum Geologists Bull.*, v. 45, pp. 1810-1846.

WELLER, S. and S. ST. CLAIR (1928). Geology of Ste. Genevieve County, Missouri: *Missouri Bureau Geology and Mines*, 2nd Ser. No. 23, 352 p.

WILMANN, H. B., E. ATHERTON, T. C. BUSCHBACH, C. COLLINSON, J. C. FRYE, M. E. HOPKINS, J. A. LINEBACK and J. A. SIMON (1975). Handbook of Illinois stratigraphy: *Illinois State Geol. Survey Bull.* No. 90, 261 p.

PLATE 1

Group 1. Calcisiltites (including Stromatolites)

A. Microfacies 60. Stromatolitic bioconstructed limestone with poorly defined and crinkled algal mats, intermat calcisiltite with rare minute bioclasts of crinoids and small fenestral cavities filled with microsparite. Pyrite pigments are concentrated in the algal mats.

B. Microfacies 50. Laminated calcisiltite with abundant small euhedral anhydrite crystals and common pyrite pigments. The calcisiltite is regularly laminated, bituminous and slightly pelletoidal. The anhydrite crystals may sometimes interfere forming poorly developed rosettes (upper right).

Group 2. Pelletoidal Bioclastic Calcisiltites, Mud-Supported Biocalcarenite and Bioaccumulated Limestone

C. Microfacies 37. Pelletoidal bituminous and spiculitic calcisiltite with common monaxonic sponge spicules, calcispheres and ostracods. Minor small crinoids often with syntaxial rim cement are associated with rare patches of sparite cement.

D. Microfacies 36. Poorly sorted mud-supported biocalcarenite with bituminous calcisiltite matrix. Large crinoids, bryozoans, echinoid spines, brachiopods and ostracods are irregularly distributed by bioturbation. Pyrite pigments are common.

E. Microfacies 35. Bioaccumulated bryozoan-brachiopod limestone with pelletoidal calcisiltite matrix. Large subparallel elongate bryozoans and brachiopods are common. The matrix is a pelletoidal calcisiltite with common minute bioclasts of crinoids, brachiopods and bryozoans.

Group. 2. Mud-Supported Pelletoidal Biocalcarenites and Grain-Supported Pelletoidal Biocalcarenites

F. Microfacies 33. Grain-supported crinoid-bryozoan *Endothyra* calcarenite with bioclastic matrix. Sand-sized bryozoans, crinoids and small benthic foraminifers are set in a matrix of bituminous calcisiltite with abundant bioclasts (crinoids, bryozoans, ostracods and brachiopods). Small benthic foraminifers are common in left half of photomicrograph. The large bryozoan fragments (upper right) have their zooecias infilled with sparite cement.

G. Microfacies 23. Grain-supported, fine grained pelletoidal crinoid-bryozoan calcarenite with calcisiltite matrix and sparite cement. Small rounded lithic pellets of calcisiltite are abundant and associated with crinoids and bryozoans. The rock is moderately well sorted and fairly well laminated. Pressure-welding of the pellets is clearly displayed.

Group 2. Grain-Supported Biocalcarenites with Calcisiltite Matrix and Sparite Cement to Intraclastic or Pelletoidal Biocalcarenites with Sparite Cement

H. Microfacies 22. Grain-supported intraclast-crinoid-bryozoan calcarenite with sparite cement and local pressure-welding. The rock is moderately well sorted. The cement consists of syntaxial overgrowths on crinoids. The elongate bioclasts (echinoid spines, crinoids and bryozoans) impart a faint lamination to the rock.

All photomicrographs: plane polarized light.

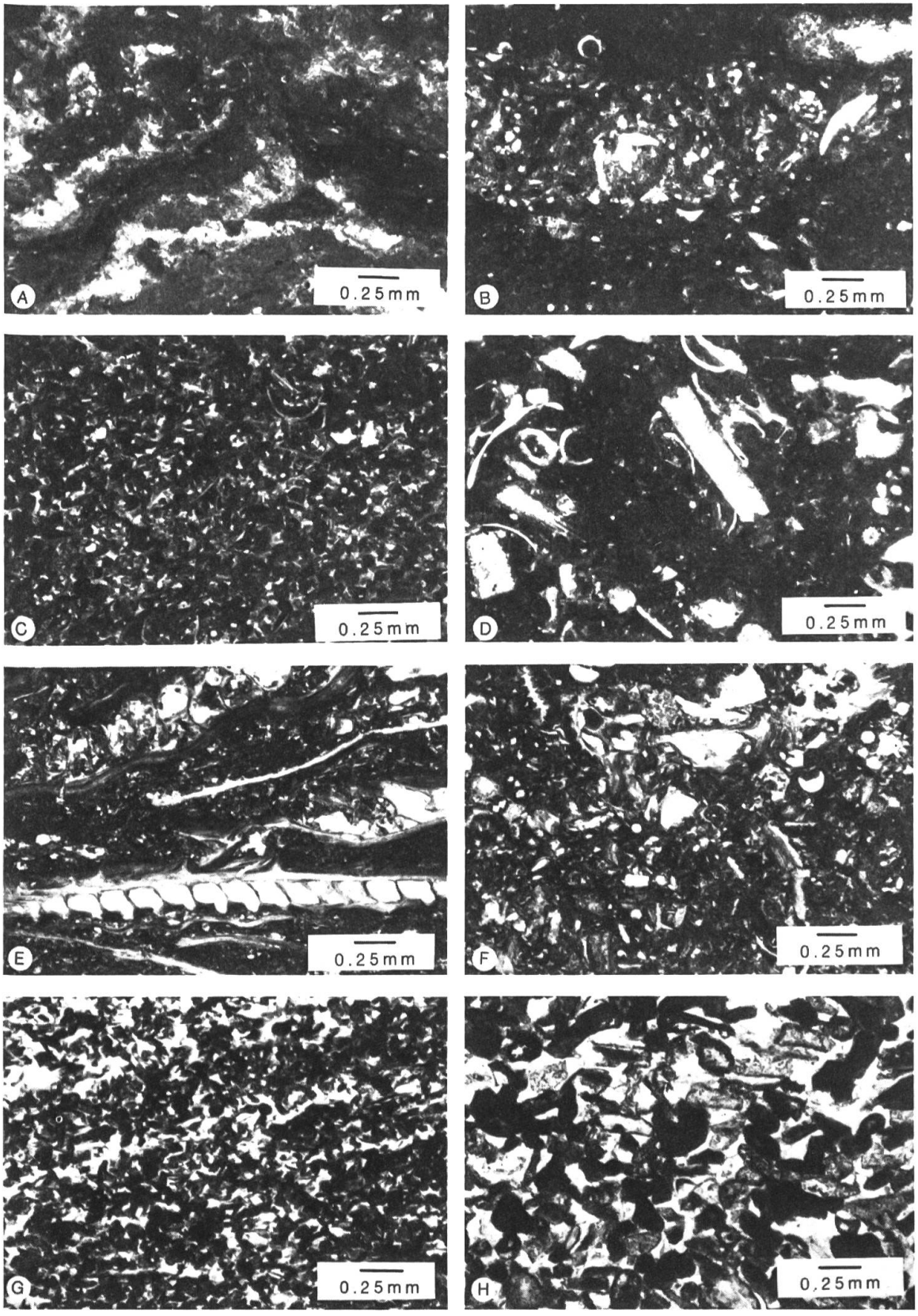

PLATE 1

PLATE 2

Group 2. continued

A. Microfacies 31. Grain-supported crinoid-bryozoan calcarenite with sparite cement and common pressure-welding. The crinoids have common syntaxial calcite overgrowths grading into equant cavity filling sparite cement. The rock is slightly laminated as elongate bioclasts are subparallel.

B. Microfacies 21. Coarse grain-supported crinoid-intraclast-bryozoan biocalcarenite with sparite cement. Syntaxial calcite overgrowths around crinoids are associated with local pressure-solution and interparticle equant calcite cement. Rare echinoid spines (center of photomicrograph) are present.

Group 3. Grain-Supported Oolitic Biocalcarenite with Calcisiltite Matrix to Grain-Supported Oolitic Biocalcarenites with Sparite Cement

C. Microfacies 11. Grain-supported ooid-crinoid-intraclast calcarenite with sparite cement and local pressure-solution. Ooid cores are crinoids, bryozoans and intraclasts. Intergranular cement consists mostly of cavity filling equant calcite with some overgrowths around crinoids.

D. Microfacies 10. Grain-supported and pressure-welded oolitic calcarenite with sparite cement. Ooids are abundant, well sorted and set in a cement of intergranular sparite calcite mosaic. Pressure-solution contacts between ooids are widespread (chain ooids along left edge of photomicrograph, deformation of ooid right of center). Nicols half crossed.

Diagenetic Sequence

Marine Phreatic Environment

E. Micritization of margins of a green algal fragment. The micritized envelope is fairly thick, broken in places and is now infilled with microsparitic calcite.

F. Early compaction II of well formed ooids causing local solution of thin isopachous rim cement. Geopetal pelletoidal internal sediment is present between ooids and is overlain by freshwater phreatic sparite cement.

G. Early compaction II also causes deformation and strong interpenetration of ooids with thin isopachous rim cement. Minor spalling of ooid cortical layers is present. Intergranular spaces are filled by geopetal pelletoidal internal sediment overlain by freshwater phreatic calcite cement.

Marine Vadose Environment

H. Development of euhedral crystals of anhydrite (anhydrite I) by replacement of bituminous calcisiltite. Notice inclusions of unreplaced matrix. Subsequent marginal calcitization (freshwater phreatic) is visible in crystal extinction in center of photomicrograph (nicols half crossed). All other anhydrite crystals are entirely calcitized.

All photomicrographs: plane polarized light (except D and H, half crossed nicols)

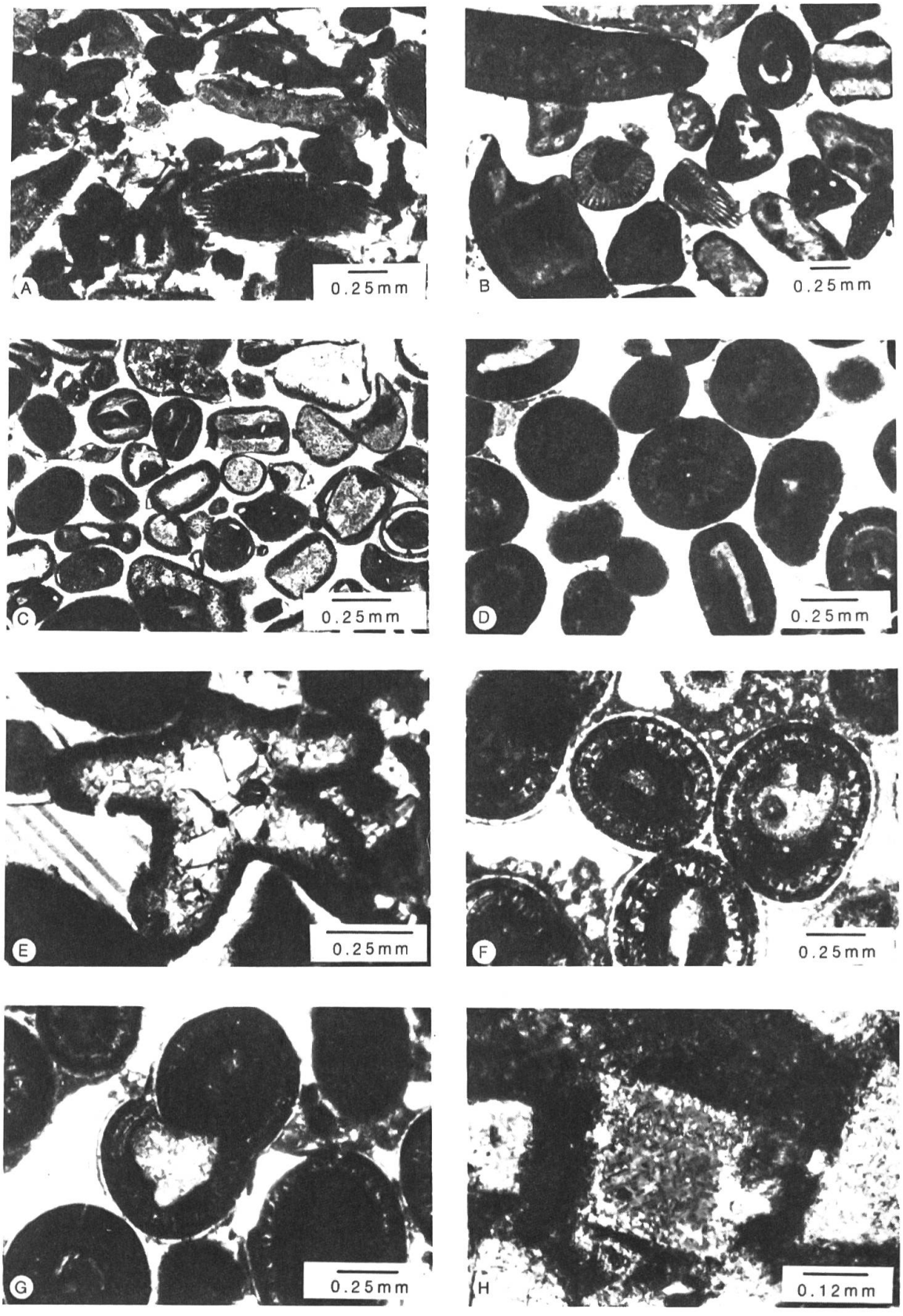

PLATE 2

PLATE 3

Diagenetic Sequence

Undersaturated Freshwater Phreatic Environment

A. Early fracturation of ooids after deposition of geopetal internal sediment. The thin fractures cut across ooids, isopachous rim cement and geopetal internal sediment. The fractures are filled with microsparitic cement from the saturated freshwater phreatic environment. The remaining intergranular spaces are filled with coarser freshwater phreatic cement.

Saturated Freshwater Phreatic Environment

B. Syntaxial calcite overgrowths enclosing bryozoans developed around crinoids and forming an interlocking mosaic (crossed nicols).

Mixing Marine Freshwater Phreatic Environment

C. Pervasive silicification resulting in growth of secondary euhedral quartz crystals within an ooid core and inner cortical layers. Notice 'ghosts' of the cortical layers inside the crystal (crossed nicols).

Burial Environment

D. Burial dissolution of intergranular sparite cement creates secondary porosity (3.6%) filled with blue epoxy (appearing gray, arrows).

E. Partial anhydrite replacement of bioclasts (crinoids and bryozoans), ooids and sparite cement (arrows). The anhydrite is subhedral to euhedral (anhydrite II), crossed nicols.

F. Euhedral crystals of anhydrite replacing a partially silicified bryozoan showing that the second phase of anhydritization follows silicification.

G. Late burial fracturation and sparite cementation of fractures. Notice also partial anhydritization (arrow) of fracture-filling calcite cement by bladed anhydrite III (crossed nicols).

H. Late dolomitization by saddle dolomite in cavities (fractures) in a pelletoidal calcisiltire. Upper right and upper left show margins of the fracture (crossed nicols).

All photomicrographs: crossed nicols (except A, D and F, plane polarized light).

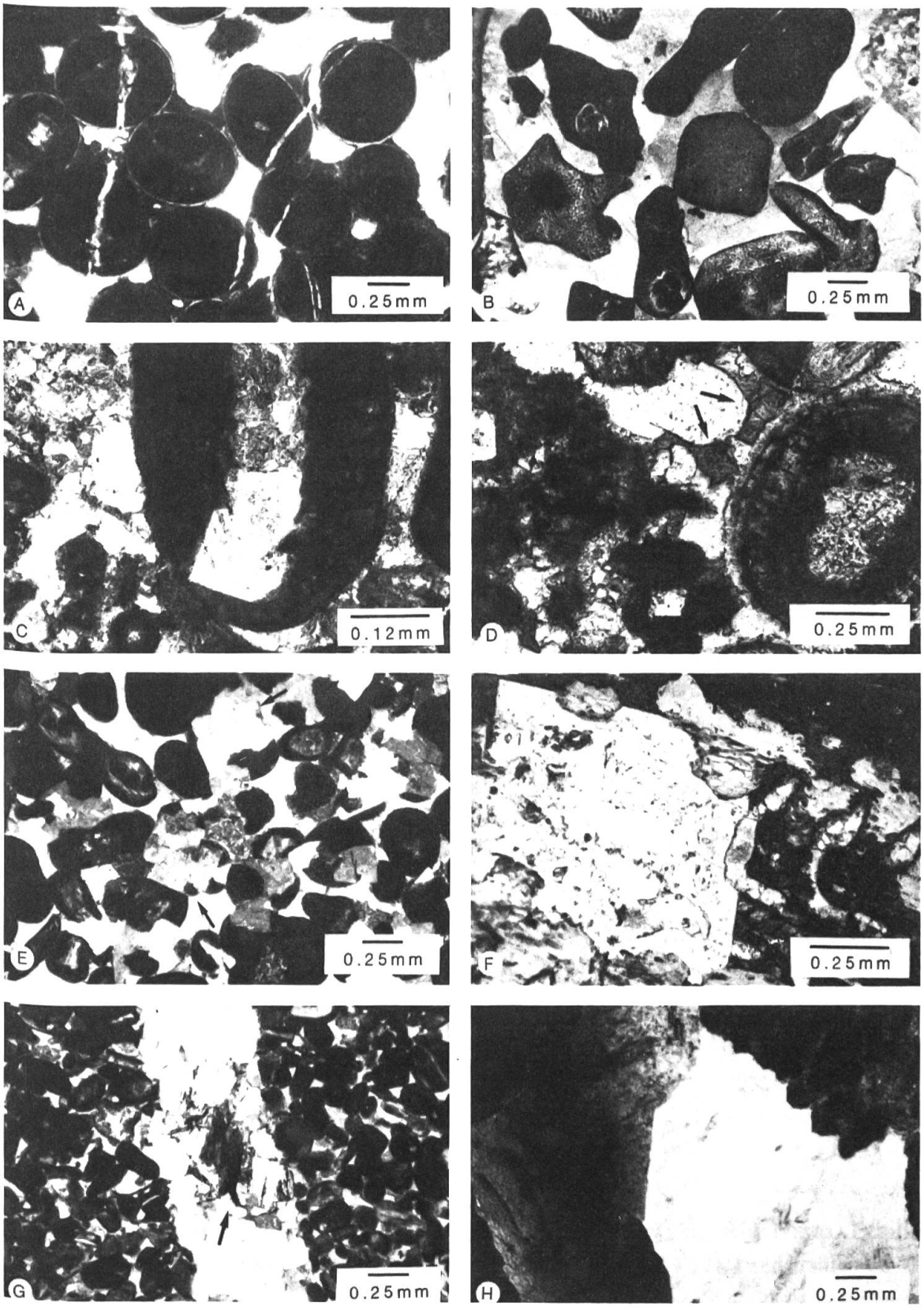

PLATE 3